Inertial rotation and matrix interaction effects on the EPR spectra of methyl radicals isolated in 'inert' cryogenic matrices

2009 J. Phys.: Condens. Matter 21 103201

(http://iopscience.iop.org/0953-8984/21/10/103201)

J. Phys.: Condens. Matter **21** (2009) 103201 (21pp) doi:10.1088/0953-8984/21/10/103201

TOPICAL REVIEW

Inertial rotation and matrix interaction effects on the EPR spectra of methyl radicals isolated in 'inert' cryogenic matrices

Nikolas P Benetis[1] **and Yurij Dmitriev**[2]

[1] Nikolas-Ploutarch Benetis, Department of Pollution Control, Technological Educational Institution, TEI, West Macedonia, Kozani 501 00, Greece
[2] A F Ioffe Physico-Technical Institute, 26 Politekhnicheskaya Street, 194021 St Petersburg, Russia

E-mail: niben@teikoz.gr and dmitrievyurij@gmail.com

Received 15 September 2008, in final form 7 December 2008
Published 5 February 2009
Online at stacks.iop.org/JPhysCM/21/103201

Abstract
The CW-EPR lineshapes of methyl and small methyl-like radicals trapped in noble gas matrices at liquid He temperatures are substantially different from the expected classical EPR spectra. At low temperatures they show small or negligible anisotropy in studies using different experimental techniques and have a temperature dependence that differs from systems whose motional dynamics is diffusion controlled. At liquid He temperatures, before the Boltzmann statistics take over in the classical high temperature realm, the spectral intensities are dominated by quantum statistics. These properties, which were obtained experimentally at temperatures about 5 K and lower, and up to about 20 K, can be attributed to quantum effects of inertial rotary motion and its coupling to the nuclear spin of the radical. Methyl-like radicals have nuclear-exchange symmetry and contain the lightest possible isotopes, protons, and deuterons. In the ideal case of absent radical–matrix interaction, the methyl rotation about the central heavier carbon atom guaranties minimal moments of inertia. However, the theoretical interpretation of the above effects and other related quantum effects, as well as recognition of the important physics which lead to them, is not a simple matter. The literature accumulated on the subject over the years is successful but contains several unresolved questions. Recently obtained spectra of methyl radicals in Kr, N_2 and CO matrices, which are less inert than the smaller noble gas Ar, were shown to exhibit greater, but certainly slight, overall anisotropic spectral features while in earlier experimental studies the anisotropy was practically absent. Even gases of smaller radii such as Ne and H_2 at liquid He temperatures show interesting differences as hosts of methyl radicals compared to Ar. Investigation of other possible causes of this difference, not excluding the experimentally controlled ones related to the sample preparation and the MW power saturation of the CW-EPR measurement, were conducted in this work.

(Some figures in this article are in colour only in the electronic version)

Contents

1. Introduction

Planar, methyl-type $^{\bullet}CX_3$ (X = H, D) rotor radicals in noble gas matrices of Ne, Ar and Kr at liquid He temperatures can, under certain conditions, be considered as pure quantum rotors that occupy the first few rotational levels [1]. The rotational constants of the methyl rotor is of the order of 7 K, thus being significantly larger than the rotational constants of regular 'heavy' molecules with lower symmetry and heavier peripheral X atoms than H and D. (We will occasionally refer to these systems as ultra-light and highly symmetric quantum rotors since they bear such properties if the interaction of the radical with the matrix is not large enough to quench rotation [2].)

The fundamental properties of the pure quantum-rotor model applied to experimental EPR lineshapes of the methyl radical were studied earlier [1]. Theoretical examination of the quantum effects on the EPR spectra of selected methyl-type radicals and variations of such spectra for radicals with symmetry smaller than D_3 was performed, utilizing a three-dimensional (3D) free rotor motional model. Thus, surprisingly enough, even the experimental spectra of isotropically mixed rotors CH_2D and CHD_2, which have solely fundamental D_2 symmetry, were also characteristically affected by exclusion of certain EPR transitions [1]. As was explained in that work, the basic reason for the observed effects was the fundamental symmetry operation of the exchange of the two identical proton or deuteron nuclei of the molecules by C_2 rotation, considering that they are fermions and bosons, respectively.

The EPR spectra of $^{\bullet}CH_3$ obtained in the noble gas matrix of Ar were interpreted according to group theoretical considerations. These spectra, recorded at temperatures close to 5 K, displayed typical quantum effects due to the spin-rotation coupling[3]. In the spectral simulations, this coupling was represented by an anisotropic hyperfine interaction of the unpaired p_z electron with the peripheral H or D nuclei. The corresponding mixed spin-rotation Hamiltonian contained explicitly molecular angular momentum operators and electronic and nuclear spin operators [1, 3]. The agreement of the experimental EPR spectra with a pure quantum-rotation model was satisfactory but not always.

Under conditions of weak coupling of the rotational degrees of freedom with the 'lattice', which are expected to prevail at temperatures lower than 5 K, the thermal energy of the matrix atoms is unable to excite the first non-trivial rotational level (the first level above the ground rotational level with angular momentum $J = 1$). The experimental EPR lineshapes at this low temperature were determined by the special properties of the quantum rotor at the ground rotational level with zero angular momentum ($J = 0$) [1]. Certain questions were not possible to resolve in that study.

It was, for example, theoretically estimated that the quantum effects should become of minor significance first at temperatures between 40 and 60 K, giving place to classical effects of stochastic motion at even higher temperatures. However, the experimental EPR spectra showed the effect of random rotary motion sometimes already at 10–15 K, as in the case of deuteron-substituted methyl, and in more recent experiments classical characteristics of EPR lineshapes appeared at even lower temperatures.

Recent results of $^{\bullet}CH_3$ radicals[4] in a Kr matrix by Dmitriev [4] showed unexpectedly that the E-lines emerged at a temperature as low as 4.1 K and persisted even down to 1.5 K. Description and interpretation of the phenomenon, including saturation conditions of the EPR acquisition, are to be found in the section about the Kr–CH_3 system. Briefly, we suggest that the E-line series originate from EPR spectra of CH_3 radicals trapped in the matrix in positions with axial symmetry.

Very recently, the anisotropic spectrum for methyl radicals in solid Ar was observed at temperatures above 14 K in condensation experiments by Popov *et al* [5] and they mentioned that the properties of the rotors were to be deduced from the EPR spectra. They use highly specialized group theory to extract the effects of the crystal lattice but they consider the system at temperatures greater than 14–35 K where earlier studies showed that the quantum effects have already almost disappeared.

The motional dynamics of methyl rotors has been found to be important in understanding the experimental EPR lineshape, ESEEM, and ENDOR properties in solid state for experiments performed at very low temperatures [6]. In ESE studies of methyl-substituted nitroxides it was obvious that nuclear and electron spin relaxations were affected very distinctly by the quantum properties of methyl rotation in excess of the effects of classical relaxation theory [7–9]. However, the experimental facts about the effect of the hindered internal rotation of methyl fragments in nitroxides have not been treated theoretically in detail so far.

It looks reasonable to suggest that the EPR lineshapes of trapped methyl radicals in solid matrices are governed by the magnitude of the radical/matrix–particle interaction. Some hints about how inert a matrix is may be obtained from the EPR data of the simplest matrix-isolated objects, the H atoms.

Comparing the effects of the H_2 and Ar matrices on the hfi (hyperfine interaction) constant and g factor of a trapped hydrogen atom (usually called matrix shifts), the shifts are smaller in H_2 than in the Ar matrix. This result is in accordance with the fact that the gas kinetic diameter of H_2 is smaller than that of Ar, see table 1.

[3] Spin-rotation coupling is used in two different senses in the literature: (a) in high temperature spin relaxation theory it means the coupling of the electron spin with the angular momentum of the rotating molecular species. (b) In treating quantum rotors here it means the mixing of the angular momentum of the rotating molecule with the nuclear spin degrees of freedom through an orientation-dependent hf coupling.

[4] For simplicity the CH_3 radical will be denoted later without the dot for the unpaired electron.

Table 1. Molecular gas kinetic diameters determined by viscosity measurements from Malkov *et al* [31] and Deshman [46].

Gas	Xe	CO_2	CH_4	Kr	Air	N_2	CO	Ar	O_2	NH_3	H_2	Ne	He
Diameter (Å)	4.91	4.65	4.19	4.15	3.74	3.70	3.70	3.67	3.64	2.97	2.75	2.60	2.18

Based on the gas kinetic diameters, one may expect a further decrease of the matrix effect for H in Ne compared to the H_2 matrix. Although the situation is not clear enough for the H–Ne pair, as can be deduced from the EPR literature on H trapped in Ne, evidence is available suggesting that the shifts are substantially smaller for substitutional H in Ne compared to the substitutional H in H_2.

Hence, according to the EPR results for the H atom in Ar, Ne and H_2 and the gas kinetic diameters of these matrix particles, the 'inertness' of a matrix tends to increase going along the sequence Ar, H_2, Ne of decreasing radii.

On the other hand, H_2 and Ne are in a kind of a particular position concerning these properties and the conclusion is not as obvious in the case of trapped CH_3 radicals. Indeed, in spite of the fact that the EPR spectrum of the CH_3 radical shows anisotropy in the Ne matrix [10] the anisotropy was not obvious either for the n-H_2 gas[5] matrix [11] or for the p-H_2 matrix. Actually in the latter case of p-H_2, the anisotropy of the EPR lineshape of methyl was very small and was easier to prove compared to the broader spectra in n-H_2 [12].

One obvious reason for that was the absence of the superhyperfine interaction from the non-magnetic, antisymmetric state of the protons in p-hydrogen. Furthermore, this result suggests that the intensive tunneling motion of matrix particles in the case of the H_2 matrix enables more free rotation of trapped CH_3 radicals.

Concluding this introduction, it has to be pointed out that due to quantum effects the anisotropy of all the cases studied here was present as line asymmetry and line splitting, i.e. it was extremely small, in clear contrast to the classically expected powders!

The aim of the present work is to compare new experimental EPR spectra of methyl radicals recorded in cold matrices of different monatomic and diatomic gases of various polarities and prepared under different techniques compared to older studies. More generally an attempt will be made to clarify some of the remaining peculiarities of the low temperature EPR spectra of light and symmetric radicals in nearly inert, very cold matrices.

Finally, let us in the following summarize certain unresolved questions, with the purpose of giving us the opportunity to answer them later in this work.

- Some of the apparent features of the low temperature EPR spectra of the methyl radical could be explained with high temperature theory, involving classical rotation. Thus the shift of the E-lines compared to the A-lines and the differential broadening of the CH_3 spectra were already affected by diffusional properties of motion at 15 K.
- It is not certain if the larger space between the larger gas molecules of a certain matrix, which probably allowed more free motion for the methyl radical, led to smaller anisotropy or if this effect may cancel out, or even be inverted, by the larger van der Waals forces of the larger matrix molecules. More experimental work on this system is currently in order.
- Neither the CH_4 impurity nor imperfections of the structure of the solid matrix can explain the spectral asymmetry of the CH_3 radical generated from CH_4. Considering that the matrix plays an important role in the sample preparation, further research is required to resolve this problem, maybe including the formation, the deposition of the matrix and the interaction of the radicals with the matrix molecules.

[5] The n-H_2 (normal hydrogen) contains 75% ortho o-H_2 and 25% para p-H_2 molecules.

2. Theory of methyl rotors

Although this paper concerns the EPR spectra of the CH_3 radicals in inert and less inert gas matrices at liquid He temperatures, it is instructive for the purpose of comparison to review first the basics of the hindered –CH_3 rotor as a fragment of a larger molecular entity.

2.1. Hindered rotation of 'light' C_3 molecular fragments

The first studied tunneling $>C^{\bullet}_{pz} - CH_3$ rotors were C_3 fragments of small organic acids with beta-protons with respect to the p_z orbital on the carbon of the carboxyl group, such as methyl malonic acid studied by Freed [13] and by one of us [3].

Quantum effects of the above rotors can be summarized as the E-line splitting and the tunneling satellites.

The E-line splitting has major and minor consequences. Its occurrence is connected with the thermal activation of the degenerate $|l| = 1$ level. The major effect is the transformation of the well-known lowest temperature quartet of equal intensity of the lowest $l = 0$ rotational level into a septet. Furthermore this septet is characterized by a slight central E-line splitting and a corresponding outer E-line shift, seen in the simulated spectrum of figure 1. This is the minor effect of the E-line splitting which leads to the unequal spacing of the septet.

When the tunneling frequency is comparable to the hf (hyperfine) splitting, forbidden transitions also appear outside the wing of the main EPR spectrum. The two weak formations, so-called tunneling satellites (see figure 1), are a direct consequence of the mixing of the A-and E-blocks of the rotational Hamiltonian [14].

The simulation in figure 1 was performed without approximations of the rotational part, of the hf coupling or symmetry, but very similar results could be obtained analytically using the I, S secular spin-Hamiltonian [14]. Thus the new most intense central line is the result of the two superimposed degenerate E-lines at the rotational $l = \pm 1$

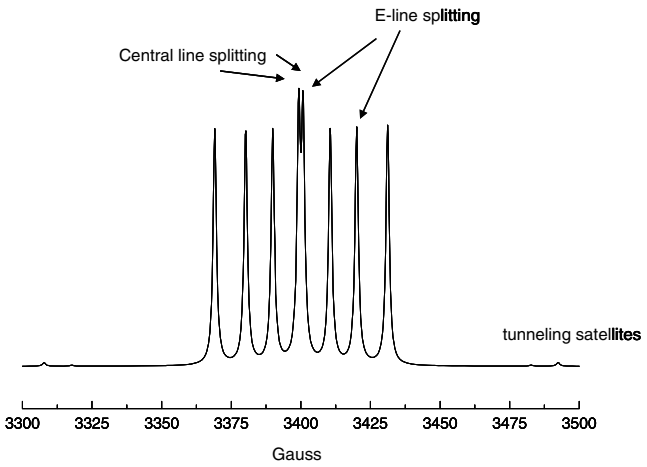

Figure 1. Simulation showing the E-line splitting, central line and the tunneling satellites. This simulation was performed without approximations of the rotational levels or symmetry. (See [3] for a systematic experimental temperature dependence of the EPR spectra of the tunneling methyl radical along with simulations, and [14] for the detailed structure of the tunneling satellites.)

Table 2. The motional variables of the internal uniaxial rotation of the $–CH_3$ and $–CD_3$ molecular fragments for different potential barriers V_3 hindering the motion. The rotational constants used for the computations were 7.605 and 3.8014 K for proton and deuteron, respectively.

Rotor and rotational constant (K)	V_3 (K)	Ground level energy (K)	Tunneling energy (K)
$–CH_3$	0.001	0	7.605
7.605	50.0	—	5.195 53
	100	—	2.605 26
	200	53.35	0.688 26
	650	100.9	$7.255\,8 \times 10^{-3}$
$–CD_3$	0.001	0	3.801
3.8014	200	39.06	3.506×10^{-2}
	650	72.36	3.7862×10^{-5}

levels split by the secular hf interaction. The E-line splitting was first discovered by Freed [13] who explained in this way the reason for the peculiar He temperature septet of the methyl radical at lowest temperatures.

The dependence of the tunneling frequency on the potential barrier and the values of the rotational constants for the methyl fragments containing H and D obtained (as a by-product) during the same simulation procedure are given in table 2. The experimental couplings from high temperature spectra are $a_H = 25$ G and $a_D = 3.88$ G. According to the ratio $\gamma_H/\gamma_D = 6.512$ and considering the a_H given above we calculate $a_D = 3.84$ G, which shows that the experimental rotor is a β-deuteron-CD_3, at least at high temperature.

In contrast to the above fully quantum mechanical treatment of the rotation, an effective spin-Hamiltonian operator, including the tunneling splitting in analogy to the Heisenberg exchange case, was given by Apaydin and Clough [15] and it was used by Mottley *et al* [16] to simulate the effects of the coherent and random rotation of the methyl group in ELDOR.

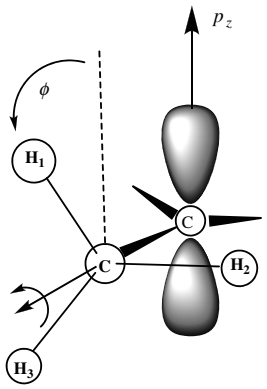

Figure 2. The configuration of a beta-proton methyl rotor as a fragment of a larger paramagnetic entity.

Articles mentioning the small anisotropic contribution of the hf interaction for the methyl protons are very rare in the literature [6]. The observed unusual quantum effects in methyl fragments of larger radicals were attributed to the orientation-dependent isotropic hf interaction of the protons, in combination with a C_3 potential hindering the rotation. As seen in figure 2, the internal rotation of the methyl fragment changes the conformation of the radical and affects the hf interaction of the three protons, depending on the dihedral angle H–C–C–p_z formed by each of them [3]. (A cosine square law of the dihedral angle is involved.)

The usual explanation of the lacking anisotropy is the averaged hfi by fast rotation of the methyls as fragments of the larger molecular unit. The rotary motion of the above-discussed methyl fragments was furthermore considered to be substantially hindered also by intermolecular forces, depending on the state/phase of the solid (crystal lattice), represented by a total potential barrier of the order of 1000 K. For barriers about 600 K the methyl rotor could tunnel through the barrier giving very particular EPR lineshapes.

Cases of much smaller barriers, e.g. in toluene with a barrier of 6.8 K (!), should correspond to almost free rotation. Also much higher potential barriers than 1000 K, up to 2000–3000 K with strongly hindered rotation, also exist where the protons of the methyl perform torsional oscillation [17]. (The high value of 3000 K is usually referred to the methylene fragment $–{}^{\bullet}CH_2$.)

The strongly hindered methyl performs torsional oscillations, where the motion is not possible to stop in the classical meaning, i.e. by freezing of motion at very low temperature. The potential energy is instead transformed back-and-forth to kinetic energy. Those quantum systems perform zero-level oscillations if the barriers are too high, or otherwise the protons tunnel (coherently) to the adjacent wells [2, 13] for intermediate barriers. In the case of really low barriers compared to the splitting of the pure rotational states, such as for 'light' protonated methyl rotors in frozen inert gases, the rotation stops as per the definition when only the lowest rotational level with zero angular momentum ($\ell = 0$) is populated. The EPR spectra of the stopped quantum rotors are characteristic [1], i.e. they consist of four equal-intensity lines as shown in figure 3(b)

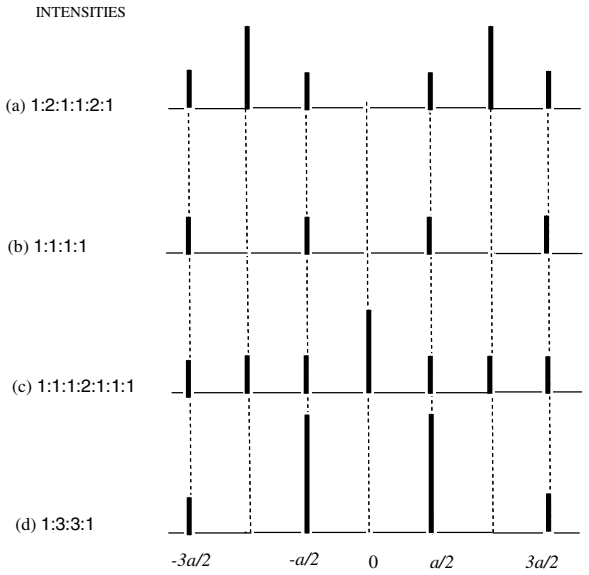

Figure 3. Basic EPR stick spectra for a hindered beta-proton methyl rotor of C_3 symmetry with isotropic hf coupling along with the appropriate limiting conditions for the motion, see text for details. (a) Stopped classical rotor ($\tau_{exch} \to \infty$). (b) Stopped quantum rotor ($\ell = 0$) or strongly hindered diffusional rotor. (c) Tunneling quantum rotor (superposition of $\ell = 0$ and ± 1 rotational levels). (d) Fast classical ($\tau_{exch} \to 0$) and very rapid high energy quantum rotor (high rotational quantum numbers ℓ). The quantum mechanical z-projection quantum number of the rotational angular momentum is denoted by ℓ. Notice that the stopped quantum rotor in (b) requires negligible barrier and that it is also obtained for the classical treatment of motion [19].

and occur at the lowest liquid He temperatures where adequate thermal excitation is lacking.

Freed [13] was the first to recognize and interpret the quantum effects of spin-rotation coupling on the CW-EPR spectra of a hindered methyl rotor at low temperatures and derived the tunneling rotor septet seen in figure 3(c). In the same figure two more characteristic cases of experimentally obtained spectra are shown, in addition to the above two, using as a model the identical methyl fragment for different thermodynamic conditions. The approximate stick spectra of this figure have been computed using identical magnetic parameters. The underlying physics for the differences are briefly explained in the legend of figure 3.

Further, two more characteristic features, i.e. the E-line splitting leading to central line splitting and the outer-line shift, as well as the *tunneling satellites* were explained and the conditions for obtaining these features were studied. In the simulated spectra of figure 1 one can see actually both the above effects. (For details of the simulation see [14].)

To our knowledge, there is not as extensive a literature about the deuteron $–CD_3$ as there is for the proton $–CH_3$ rotor spectrum and sometimes there are contradictory interpretations in the literature [18, 14]. That was one of the reasons that we presented earlier the counterpart to Freed's three β-proton-CH_3 quantum septet, i.e. the corresponding quantum spectrum of the radical for three peripheral deuterons ($–CD_3$) with spin $I = 1$ [14]. In that paper we reported the approximate transition frequencies and the corresponding intensities of the appropriate spin-rotation Hamiltonian, as well as accurate numerical simulations of the deuteron rotor spectra, expanding the tunneling theory to beta-deuteron methyl rotors.

As will be seen further, two characteristics of the beta-proton methyl fragment's EPR are missing from the free 3D rotors isolated in noble gas matrices, namely the E-line splitting and the tunneling satellites.

The E-line splitting was shown to be the exclusive property of the doubly degenerate $l = \pm 1$ rotational level. The hf interaction, being proportional to $\cos^2 \varphi$, can be separated into three terms corresponding to the totally symmetric A and the $E^{\pm}$ irreducible representations of the C_3 group. Due to this particular form of the isotropic hf interaction of the $–CH_3$ fragment only levels with $\Delta l = \pm 2$ can be coupled but no higher. This splitting must thus be absent for all the higher rotational levels with $|l| > 1$.

However, such an angle dependence is missing from the hf interaction of the free 3D methyl rotors where the hf interaction is anisotropic in the regular sense. To make this difference clear, the hf interaction of β-proton methyl fragments is isotropic in the sense that it is independent of the field orientation. However, it is modulated by the rotation of the methyl fragment in the molecule along with the conformation changes which this internal motion brings about. It differs thus significantly from the anisotropic hfi of the 3D methyl rotors, where the rank-2 hf tensor of each alpha-proton is modulated by the overall rotation of the radical.

2.1.1. Classical effects of motion. The quantum effects of the rotary motion of methyls on the EPR spectra discussed above were normally important and could be observed at the lowest experimental temperatures.

One has to point out the significant differences between the inertial and the diffusional limits of the motional dynamics for internal rotation of the methyl-type fragments. Thus for the high temperature diffusion limit the isotopic substitution does not alter significantly the thermal activation parameters of the Arrhenius type. This is in contrast to the regime of inertial rotation that is controlled by quantum effects at very low temperatures close to 5 K and sometimes up to 20–30 K. There, the dynamics of deuteron-substituted methyl have very different characteristics compared to regular methyl as was shown above and will be further analyzed for the 3D methyl rotors. We anticipate the cause of this difference to be further explained by the quantum statistical properties of protons and deuteron, being fermions and bosons, respectively.

Thus, each of the following pairs of rotatable molecular fragments, ($–CH_3$, $–CD_3$) and ($–^{\bullet}CH_2$, $–^{\bullet}CD_2$), displayed almost identical barriers at high temperature in spite of the different moments of inertia.

(i) The methyl fragment CH_3 and the deuterated analogue CD_3 in acetic acid anion radicals [20]: obviously the moment of inertia is not involved. The rate of rotation in the first pair was found to be $k_H = 3.3 \times 10^{11}$ Hz $\times$ exp(2.2 kcal mol$^{-1}/RT$) for proton and $k_D = 4.8 \times 10^{11}$ Hz $\times$ exp(2.5 kcal mol$^{-1}/RT$) for deuteron, in the temperature range 77–170 K, and,

(ii) The methylene and deuterated methylene fragments $-^{\bullet}CH_2$ and $-^{\bullet}CD_2$, respectively, in irradiated crystals of Zn-acetate single crystals [21].

In the second pair the temperature dependence of the rate of rotation was identical for both the proton and the deuteron fragments given by the equation

$$k = 6.7310^{12}\ \text{Hz} \times \exp(-7.17\ \text{kcal mol}^{-1}/RT) \qquad (1)$$

in the temperature range 170–300 K.

2.2. Alpha-proton methyl rotors

Several new interesting quantum effects other than tunneling were observed experimentally and were explained theoretically on the EPR spectra of methyl radicals isolated in inert gas matrices at liquid He temperatures close to 4 K [14]. With increasing experimental temperature, the lowest temperature characteristic quartet of A-lines with equal intensity is progressively enriched by the appearance of an additional E doublet. These two lines coincide almost with the two central A-lines but are slightly shifted upfield, finally reaching the magnitude of the second-order isotropic hf shift at the highest temperatures.

Compared to classical spectra the EPR lineshapes were characterized by severe distortions due to exclusion of electron spin transitions by the $\boldsymbol{D}_3$ symmetry of the methyl radical in combination with its rotation in three-dimensional Cartesian space. It was also possible to identify the observed EPR signal from a stopped methyl rotor for both the usual proton methyl radical and the deuteron-substituted CD_3 at the lowest experimental temperatures close to 5 K.

One of the obvious reasons for this behavior was the 'high' figure symmetry of the methyl radical. However, even mixed CH_2D and CHD_2 rotors with both proton and deuteron, possessing actually only fundamental $\boldsymbol{C}_2$ symmetry, showed characteristic exclusions of transitions in their EPR spectra.

In order to explain such effects, it was necessary to compute the zero-order, lowest level eigenstates of the appropriate spin-rotation Hamiltonian. In particular the subsystem consisting of the combined quantum rotation and the nuclear I-spin degrees of freedom was treated separately from the electron spin. The zero-level states of the system were symmetrized according to minimal point group $\boldsymbol{D}_3$ of the molecular figure seen in figure 4 and the exchange symmetry of identical protons or deuterons by the $\boldsymbol{C}_2$ axes. The EPR spectra obtained by the above-described simplified procedure revealed the exclusion of several EPR transitions which were forbidden by the Pauli principle.

However, apart from the quantum effects, partially classical behavior of the EPR spectrum was also observed at higher temperatures, which were attributed to matrix–radical interactions.

More clear evidence of matrix–radical interactions was reported some years ago by Dmitriev and Zhitnikov, in the form of a 'markedly' but still mildly anisotropic EPR spectrum of methyl radicals trapped in solid CO [11].

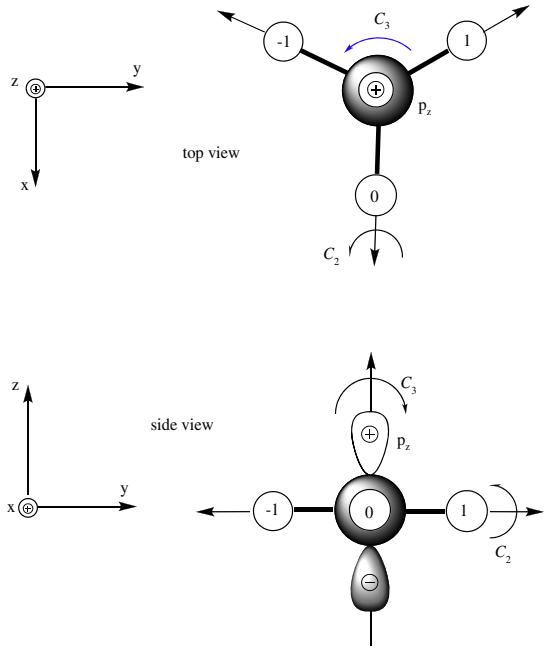

Figure 4. The model of the symmetric-top free-methyl rotor, i.e. a planar, methyl radical of $\boldsymbol{D}_3$ symmetry [22] considered in three dimensions. The rotation C_3 and C_2 axes of symmetry are indicated in the figure while the three protons are indexed by -1, 0 and 1.

2.2.1. Rotational properties of the 3D methyl. Planar methyl-type rotors XY_3 in 'inert' gas matrices can be considered as pure quantum rotors that occupy the first few rotational levels at the lowest experimental temperatures. Note that, to a first approximation, the rotor can be considered as isolated, that is no rotor–matrix interaction needs to be included in the computations.

An appropriate spin-rotational Hamiltonian for the accurate treatment of the problem has to consider the quantum mechanical rotational degrees of freedom at the same level as the electron and nuclear spins:

$$H = H_{\mathrm{R}} + H_{\mathrm{S}}^{\mathrm{Zee}} + H_{\mathrm{I}}^{\mathrm{Zee}} + H_{\mathrm{SI}}^{\mathrm{sca}} + H_{\mathrm{SRI}}^{\mathrm{dd}} \qquad (2)$$

with the kinetic energy of the free-rotation part of the Hamiltonian:

$$H_{\mathrm{R}} = \frac{J^2}{2I_{\perp}} + \left(\frac{1}{2I_{\parallel}} - \frac{1}{2I_{\perp}}\right) J_z^2 \qquad (3)$$

and considering axial symmetry of the methyl rotor.

The components of the diagonal moment of inertia tensor for the methyl radical are given by

$$I_{\perp} = 3\,m\,l^2/2 = I_{\parallel}/2 \qquad (4)$$

where m is the proton mass and l is the bond length C–H, taken here equal to 1.09 Å. This expression gives correctly the relation 2:1 for the parallel to the perpendicular component of the moment of inertia tensor, valid also generally for homogeneous disc-shape rotors, a condition which the $\boldsymbol{D}_3$ rotor satisfies.

The four terms of the Hamiltonian after the rotational part H_{R} constitute the standard Zeeman (two terms) and

the standard hf interaction (two terms), see further for explanations.

The additional $(2J + 1)$-fold degeneracy of the $|JM\rangle$ rotational level for a symmetric top is due to the independence of the rotational energy from the laboratory projection L of the angular momentum.

The motional part is assumed to consist of pure kinetic energy of revolution and vanishing potential energy. This is possible because the rotational constants become larger than 7 K, thus being higher than the experimental liquid He temperatures (see figure 5) and at the same time also a couple of orders of magnitude larger than the rotational constants of regular heavy molecules, with low symmetry.

The above facts are, of course, related to two observations and will be quantitatively discussed further in this review.

(i) The energy of the rotational levels of the free rotor are easily expressed in terms of a single rotation constant $B = (2I_{\|})^{-1}$ and are independent on the laboratory projection L of the angular momentum J:

$$E_{J,M} = B\,[2\,J(J+1) - M^2]. \tag{5}$$

These energies are doubly degenerate with respect to the molecular projection M of the angular momentum for all levels, except for the non-degenerate ground level $J = 0$.

(ii) The difference between the moments of inertia of the methyl radical for rotation about the perpendicular C_3 axis of the molecule or any of the C_2 axes in the plane of the molecule which differ by several K will be critical for the preferable rotation at small temperatures.

In the Popov/Eloranta paper [5] the larger rotational constant 11.2 cm^{-1} = 16.10 K was given. In the present study the first non-trivial rotational level obtains pure rotational energy about 20 K using a rotational constant $B = 6.775$ K. This value is smaller than the uniaxial rotational constant of the rotation of methyl fragments of larger species in the previous section due to the planarity of the 3D rotor[6], compared to the pyramidal shape of the fragment.

As seen from the energy diagram of figure 5, the perpendicular rotation to the symmetry axis, represented by the state $|J, M\rangle = |1, 0\rangle$, has greater kinetic energy than the state which represents the approximately parallel rotation, designated by $|J, M\rangle = |1, \pm 1\rangle$. This means that, for increasing temperatures from 5 K, where the system occupies the ground rotational level of the stopped rotor, the first free rotational state to be activated by thermal energy would be the slower 'parallel' rotation!

This gives the opportunity for the two perpendicular components of the hf interaction to be averaged first by the axial rotation. As is explained in detail in the next section this average gives about the magnitude of the parallel component and explains empirically the apparent isotropy of the EPR spectrum.

The hyperfine (hf) couplings are described by three regular α-proton tensors $\mathbf{A}(\Omega_\nu)$, one for each of the three nuclei

[6] About the issue of planarity of the methyl radicals, see further in the conclusions.

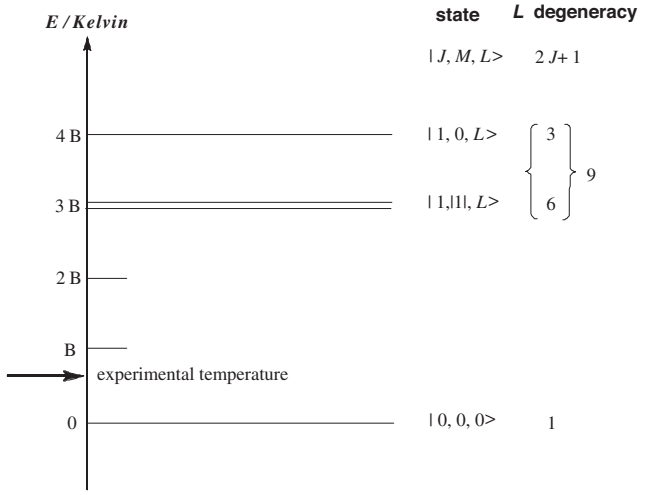

Figure 5. The two lowest rotational levels (angular momentum $J = 0, 1$) for a free, light, symmetric-top, methyl-type rotor. The rotational constant B is about 6.76 K and the experimental temperature about 5 K. The kets $|J, M, L\rangle$ of the rotational states consist of the quantum projections M and L of the angular momentum J on the molecular symmetry axis and on a laboratory frame, respectively.

enumerated for convenience as $\nu = -1, 0, 1$, see figure 4. The orientation dependence of the hyperfine interaction of each proton is expressed by the Euler angles $\Omega_\nu = (\varphi, \vartheta, \chi)_\nu$:

$$H^{\mathrm{hf}}_{\mathrm{SRI}} = \sum_{\nu=-1}^{1} \underline{\mathbf{S}} \cdot \underline{\underline{\mathbf{A}}}(\Omega_\nu) \cdot \underline{\mathbf{I}}_\nu. \tag{6}$$

Separating the trace of $\mathbf{A}$ into a scalar part and a traceless dipolar part according to $\mathbf{A} = \mathbf{1}a + \mathbf{T}$ and rewriting the tensors in standard spherical components the following relation is obtained:

$$\begin{aligned} H^{\mathrm{hfi}}_{\mathrm{SRI}} &\equiv H^{\mathrm{sca}}_{SI} + H^{\mathrm{dd}}_{\mathrm{SRI}} \\ &= -a \sum_q (-1)^q S_{-q}\, I_{q;\nu} + \sqrt{5} \sum_{\nu\, q\, r} \begin{pmatrix} 1 & 1 & 2 \\ r & q-r & -q \end{pmatrix} \\ &\quad \times \sum_{q'} D^{(2)}_{q',-q}(\Omega_\nu)\; T^{(2)}_{q'} S_r\; I_{q-r;\nu}. \end{aligned} \tag{6'}$$

Here, the isotropic splitting is $a = \mathrm{tr}\,\mathbf{A}/3$ and the non-zero spherical components of the dipolar tensor in the principal molecular frame are given by $T^{(2)}_{\pm 2} = (T_{xx} - T_{yy})/2$ and $T^{(2)}_0 = \sqrt{3/2}T_{zz}$.

The above term of the Hamiltonian in equation (6′) contains the rotational degree of freedom, the Euler angles $\Omega = (\varphi, \vartheta, \chi)$ explicitly and treats rotation at the same level as the spins are treated.

The average hf Hamiltonian for the $|JML\rangle$ rotational level is given by

$$\langle H^{\mathrm{hfi}}(\Omega)\rangle_{J\,M\,L} = [a + \tfrac{1}{2}(1 - \delta_{J,0}) C_{J\,M\,L} \cdot T_{zz}] S_z\; F_z \tag{7}$$

where $F_z = \Sigma_\nu I_{z;\nu}$ is the z component of the total nuclear spin:

$$C_{JML} = \frac{[\,3\,M^2 - J(J+1)][3\,L^2 - J(J+1)]}{J(J+1)(2J+3)(2J-1)}. \tag{8}$$

A similar type of averaging was discussed previously by Zare [23].

According to the above treatment the higher rotational levels should also display isotropic but slightly different couplings. The high-field shift of the E-doublet from the central A-lines was observed for CH_3 in Ar, see figure 6, and an explanation was attempted based on the new theory. The idea was that the E-lines allowed only in the next rotational level should also possess an isotropic but slightly different hf interaction.

Outlining the results, the quantum averaged anisotropic hf spin Hamiltonian for an arbitrary rotational level $|JML\rangle$ could be computed by equation (8). In particular, the anisotropic part of the hf interaction was eliminated at the zero rotational level while it gave, in general, a weak contribution to the scalar hf splitting for higher rotational levels. This is in agreement with the experimental facts so long as the ground rotational state dominates the spectra. In contrast, the second-order shift explained the experimental facts better than the above equation when the E-lines appear in the EPR spectrum, indicating that, when the first rotational level is activated, the classical spectral properties prevail and have to be included in the computation.

At last, a transition to broader spectra due to a classical lattice occurred when diffusion dominated. More intense interaction of the rotor with the matrix at higher temperatures can be one reason for the transition from quantum to classical behavior.

2.2.2. The hyperfine coupling. The present work deals with EPR spectra of isolated CH_3 radicals in inert gas matrices obtained in liquid He temperatures from about 1.5 K up to approx. 25 K. Methyl radicals are expected to have planar geometry, see figure 4, and therefore one should expect relatively large anisotropy in the hf interaction, since model alpha-protons exhibit approximately a rhombic hf interaction to the p_z unpaired electron with negative components $\mathbf{A} \approx (-30, -90, -60)$ MHz [24].

Actual measurements of the hf parameters of the CH_3 radical in monocrystal $CH_3COONa{\cdot}3H_2O$ by Kubota *et al* [25] gave the close result $\mathbf{A} = (-31.4, -93.9, -60.3)$ MHz. It is obvious from these values of the hf tensor that, if the averaging of the perpendicular components A_{xx} and A_{yy} occurs already at low temperatures by a fast C_3 rotation, the mean perpendicular component $A_\perp = (A_{xx} + A_{yy})/2 = -62.65$ MHz will match rather well the z component $A_\parallel = -60.3$ MHz and the residual axial anisotropy of a couple of MHz will not be easily noticeable on the EPR spectrum.

In fact, this was shown to be the case both theoretically in the previous section and in experimental EPR spectra of isolated methyl radicals in the relatively inert solid Ar matrix at about 5 K. At least no sign of the expected rhombic powder lineshape was observed in the solid [1].

In contrast, in more recent experiments of methyl radicals isolated in less inert gas matrices at equally low temperatures but under different sample preparation and saturation conditions, a varying anisotropy was observed in the EPR spectra [11]. The spectra in these cases, which will

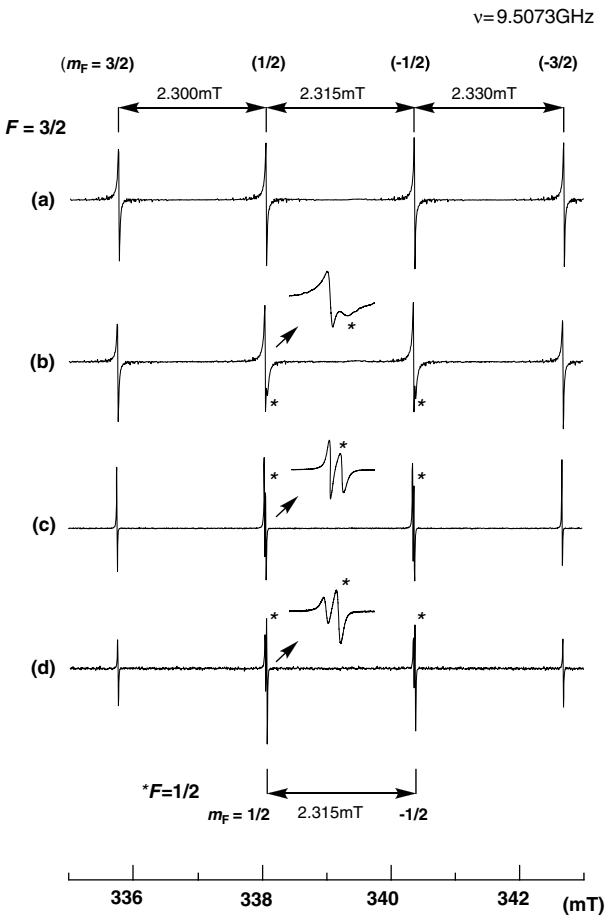

Figure 6. Temperature-dependent EPR spectra of CH_3 radical obtained in the Ar matrix containing 0.2 mol% CH_4 after x-ray-irradiation at 4.2 K from [1]. (a) 6 K: only the $F = 3/2$ quartet of 'A_1' symmetry is observable. (b) 12.0 K, (c) 20.0 K and (d) 40.0 K: two $F = 1/2$ doublets of 'E' symmetry marked as a star ($*$) increase in intensity as higher rotational levels are populated. The transitions of different symmetries ('A_1' and 'E') are separated by a small second-order shift of the isotropic part of the hf coupling.

be considered further in this text, were not that asymmetric as expected by classical considerations, however.

It was not obvious from the beginning why a much greater hf anisotropy was absent from the experimental spectra. To answer this question, the work of mainly Clough and Freed on the tunneling methyl fragment, valid for the isotropically coupled beta-protons, was successfully extended to the free rotating alpha-proton quantum rotor [1]. The new theoretical treatment involved a mixed spin-rotation Hamiltonian, as seen in the previous section, which included the well-known, very anisotropic hf interaction occurring for the alpha-protons.

Numerical spectral simulations showed that the anisotropy disappeared at the ground rotational level of the methyl radical. Based on pure quantum mechanics and group theory the results satisfied also the 'common sense' that the rotor at the ground rotational level should be stopped provided that the potential hindering the rotary motion could be ignored. Even in the improbable case that the widely published low temperature EPR quartet (four equally intense lines) represented only the visible sharp part of a spectrum prevailing over a wide baseline,

there was no doubt about its origin. It was due to the rotational level with zero angular momentum.

Common sense is fine so far that one is led to the conclusion that the zero level of rotation means stopped 'rotor' so that there is no problem for such 'rotation' to occur in the very small free space in the solidified 'gas'. It is not easy, however, to understand other consequences of the free rotor model, e.g. how the rotational averaging occurs in a stopped rotor. One should point out instead that the quantum effects that prevail at low temperatures are actually the reason and the quantum mechanical explanation of the phenomenon is in agreement with the Heisenberg principle. That is, since the angular momentum of the stopped rotor is zero the angular orientation of the rotor should be undetermined.

However peculiar the above statement appears to be it is not contradicting any of the principles of pure and basic quantum mechanics. Namely, in contrast to vibration even at zero level the quantum rotor can be stopped and, as explained above, have any orientation at any time. Actually it is found that for zero hindering potential the tunneling frequency is equal to the kinetic energy, see computations in table 2.

A careful quantum averaging of the hf term of the spin-rotation Hamiltonian at arbitrary rotational state was performed above in equation (8) showing that the anisotropic part of the hf coupling was eliminated. The effects of this averaging indicated in addition that an almost fully isotropic experimental EPR spectrum was to be expected not only in the ground rotational level but also for the higher rotational levels.

The first observation of the anisotropy of the EPR of CH_3 trapped in frozen gases by Dmitriev and Zhitnikov [11] stimulated them to test also some other matrices, like Kr [10, 11, 26], Ar [26], Ne [10], N_2 and H_2 [11].

Except for H_2, which is discussed at the end of this section, the anisotropy was detected in all matrices at liquid helium temperatures. In general, the anisotropy revealed itself as differences in amplitudes and widths of the hyperfine components, and in one case (that of the CO matrix), as line splitting. The anisotropy was also clearly observed even in the N_2 matrix, despite the strong line broadening in solid N_2 compared to CO and the atomic matrices.

The lack of anisotropy in the EPR spectrum of CH_3 trapped in the n-H_2 matrix using the experimental condensation technique used in the present and earlier work may be, in part, attributed to the rather broad lines observed; $\Delta H \approx 1$ G. The excess linewidth should be expected due to the superhyperfine interaction in a matrix formed through deposition of n-H_2 gas. However, in pure solid hydrogen, the ortho/para conversion proceeds very slowly if it is not stimulated by the trapped paramagnetic particles in the first coordination sphere. If there was no fast stimulated conversion, the linewidth would be estimated to be about 3–4 G. The greater the radius of a coordination sphere, the slower the conversion rate. We published earlier a paper devoted to the ortho/para conversion in solid H_2 stimulated by atomic nitrogen impurities [27].

2.3. The EPR spectra of 3D rotors

The quantum effects can lead to coherence between the spin degrees of freedom and rotary motion, changing the transition pattern of the EPR spectra, but usually not leading to substantial broadening. However, some years ago Dmitriev and Zhitnikov [11] observed a markedly anisotropic EPR spectrum of methyl radicals trapped in solid CO.

Summarizing the quantum effects of the EPR lineshapes for planar CH_3 and CD_3 radicals in an Ar matrix at 4–5 K, we note that they were sharp and isotropic, and that they exhibited severely distorted intensity distribution. This is a consequence of the coupling of the radical inertial rotation to the nuclear spins through the orientation-dependent hyperfine coupling. In particular the group theoretical requirements of the figure symmetry of the radical and the exchange of the identical peripheral nuclei (Pauli principle) had to be satisfied.

For example, at the lowest experimental temperature the well-known 1:1:1:1 quartet, see figure 6, was the case for CH_3 [19], and a more impressive, not reported elsewhere, single (!) central transition for CD_3, see figure 7. They both corresponded very well to the computed ideal EPR quantum transitions for the rotor being in the ground rotational level [1], stopped rotor, and they were in great contrast to an uneven 1:3:3:1 quartet for CH_3 and the septet, lowest in figure 7 for CD_3 respectively, predicted by classical high temperature behavior.

The CD_3 singlet was lately verified in deposition experiments using H_2, D_2 and Ne matrices by Dmitriev [28]. Despite more classical behavior of the CD_3-matrix system as compared with the previous study utilizing x-ray radiolysis, the singlet was clearly seen through a temperature transformation of the EPR spectrum as well as in the saturation measurements.

Dmitriev suggested a somewhat hindered rotation of the methyl radical in solid matrices, a quite different conclusion compared to the theoretical team of the Japanese group. This is conceivable since the energy of the ground rotational level is determined more efficiently by the potential than by free quantum rotation in the case of considerable potential energy. The rotor reorients in that case hopping around by tunneling, performing a quantum mechanical coherent motion that can occur in spite of the particle not having the opportunity to obtain enough thermal energy in a low temperature matrix.

2.3.1. Symmetrized basis sets. The construction of a symmetrized basis for the $\mathbf{R} \otimes \mathbf{I}$ subsystem of the quantum rotor is based on the coupling of the electron spin to the peripheral nuclei by the orientation-dependent hf interaction. It actually aims at the construction of zero-order eigenfunctions of the spin-rotation Hamiltonian of the radical. The corresponding point group involves operations that commute with the Hamiltonian, called 'the Schrödinger group' [29]. The consistency of the zero-order states to the Pauli principle for the exchange of identical particles through rotation was also assured. In particular the quantum statistics for bosons (H) or fermions (D) restricted the allowed spin-rotational states for CH_3 and CD_3 [1].

The quantum effects were most dramatic in the deuterated methyl rotor where the entire 'classically' expected EPR septet had almost collapsed to a mere singlet (!) at the lowest experimental temperature. More careful observation of the experimental spectrum obtained at 4.1 K showed that, except

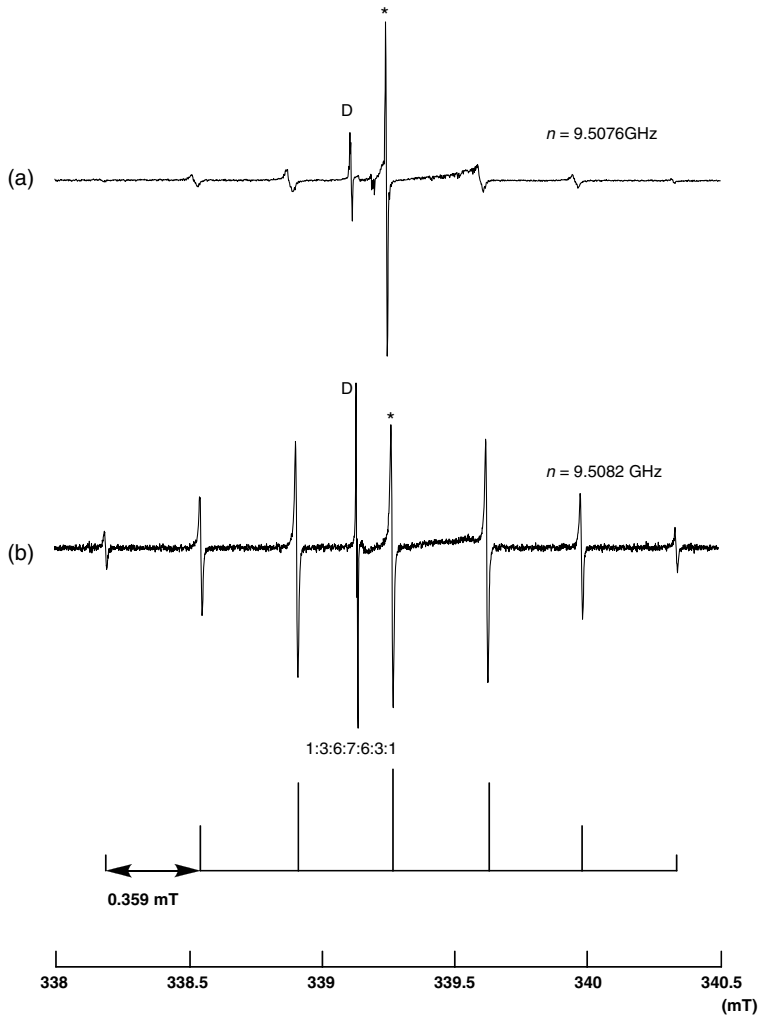

Figure 7. Upper panel: high-resolution EPR spectra of the CD_3 radical in Ar matrix at: (a) 4.1 K and (b) 25.0 K. The strong central singlet in (a), marked by star (∗), has relative intensity 105:1 to the outermost left transition. The odd line close to the center, marked by the letter D, is the deuteron atom transition ($m_1 = 0$), not relevant for this study. Lower panel: stick diagram of the classically expected septet for the radical (reprinted by permission from [1], copyright 1999, American Chemical Society).

for the abnormally strong central transition, the classical peripheral transitions were present but they were much weaker, in severe contrast to the classical septet with distribution 1:3:6:7:6:3:1. The experimental spectrum was obviously lacking the symmetric septet of the ground rotational level with intensity distribution 1:1:2:3:2:1:1. The latter should appear in the EPR spectrum of the CD_3 radical if the zeroth-order, totally symmetric nuclear wavefunction A_1 was occupied, as is the case for the β-proton rotor with $\boldsymbol{C}_3$ symmetry [14]. The only way to explain the unusually sparse lineshape of CD_3 is to admit that the only allowed state at the ground rotational level is the antisymmetric irreducible representation A_2 of the point group $\boldsymbol{D}_3$.

The equal intensity of the well-known lowest temperature quartet in the CH_3 radical [13] indicates involvement of only the rotational ground state with $J = 0$, a state referred to here as the stopped quantum rotor. The four accompanying totally symmetric A_1 states of CH_3 of the minimal $\boldsymbol{D}_3$ group are

$$\Psi^{A_1}_{000}(n, n, n) = |000\rangle|nnn\rangle \tag{9a}$$

$$\Psi^{A_1}_{000}(n, n', n) = \frac{1}{\sqrt{3}}|000\rangle[|n'nn\rangle + |nn'n\rangle + |nnn'\rangle] \tag{9b}$$

for $n = -n' = \pm 1/2$. In the above expression and in the following text a general unperturbed mixed spin-rotation $\mathbf{R}\otimes\mathbf{I}$ basis function will be designated by $\Psi^{\Gamma}_{J\,M\,L}(n_{-1}, n_0, n_1)$, where $\Gamma = A_1$ or A_2 is the overall symmetry of this function and an irreducible representation of the $\boldsymbol{D}_3$ group.

The angular momentum J, and its projections M and L, on the molecular and a laboratory frame, respectively, are the rotational quantum numbers of the basis function.

For the deuteron rotor one needs also the zero-level states given by

$$\Psi^{A_2}_{000}(\bar{1}, 0, 1) = \frac{1}{\sqrt{6}}|000\rangle\{[|\bar{1}01\rangle + |1\bar{1}0\rangle + |01\bar{1}\rangle] - [|10\bar{1}\rangle + |\bar{1}10\rangle + |0\bar{1}1\rangle]\}. \tag{10}$$

The Pauli principle requires totally symmetric wavefunctions for the exchange of two indistinguishable deuterons, in their property to be bosons. The conflict of the opposite exchange

symmetry for the deuteron can be resolved by considering also the electron S-spin degrees of freedom for the EPR supporting wavefunction of the methyl radical. It should consist of a total of three factors[7], i.e. the spin S must be included along with the rotational and the nuclear **I**-spin degrees of freedom.

The above equation displays, however, only the $\mathbf{R} \otimes \mathbf{I}$ part in the particular case that the rotational motion was at the lowest possible rotational level $J = 0$. Since the electrons are fermions the rest factors of the total state seen in the above equation must be totally antisymmetric. Furthermore since the rotational part is obviously totally symmetric the above expression contains necessarily the only possible antisymmetric deuteron spin I wavefunction.

The severely distorted EPR 'septet' of a stopped deuterated methyl CD_3 in an Ar matrix at 4.1 K is shown in the upper part of figure 7. It is compared with the classically expected septet (lower part in figure 7) which is already obtained from temperature 25 K, and higher. The classical spectrum is seen just bellow the low temperature singlet of the same figure.

2.3.2. Mixed-isotope CHD_2 and CH_2D rotors. In spite of the lower symmetry of these radicals compared to the pure H or D methyl rotors, serious symmetry restrictions for the EPR transitions of the lowest rotational levels were found.

On the other hand, the lower symmetry did not affect the treatment of the rotational degree of freedom since they are still symmetric tops. Considering the coupling of rotation to the peripheral H or D nuclei, symmetry adapted zero-level spin-rotation basis functions could be generated and used for obtaining the allowed EPR transitions.

The most interesting observation about the CHD_2 EPR lineshape at 4.2 K is the abnormally strong 1:1:1 triplet in figure 9, instead of a quintet expected for the two deuterons, see stick spectra in figure 8. The triplet can be assigned to the following three wavefunctions:

$$\begin{aligned} \psi^{\mathrm{B}}_{-1} &= [|\bar{1}\ 0\rangle - |0\bar{1}\rangle]/\sqrt{2} \\ \psi^{\mathrm{B}}_{1} &= [|0\ 1\rangle - |1\ 0\rangle]/\sqrt{2} \\ \psi^{\mathrm{B}}_{0} &= [|1\bar{1}\rangle - |\bar{1}\ 1\rangle]/\sqrt{2}. \end{aligned} \tag{11}$$

They are the only ones allowed by the Pauli principle for the lowest rotational level and correspond to the B irreducible representation regarding the C_2 symmetry of CHD_2. Only the deuteron spin projections of the nuclear I factor out of the $\mathbf{R}\otimes\mathbf{I}$ spin-rotational states at the ground rotational level $|0\,0\,0\rangle$ are given in the above expressions for simplicity.

Further, it is enough for the purpose of the present work to outline the properties of the $J = 1$ level for the particular molecular z projection $M = 0$ of the radical. (The other projections give a similar distribution.) There are six possible nuclear spin, totally symmetric combinations for CHD_2, allowed in this level.

They are

$$\psi^{\mathrm{A}}_{-2} = |\bar{1}\ \bar{1}\rangle \qquad \psi^{\mathrm{A}}_{0} = |0\ \ 0\rangle \qquad \psi^{\mathrm{A}}_{2} = |1\ \ 1\rangle \tag{12a}$$

[7] Factorization is not always possible but at least for some zero-order states.

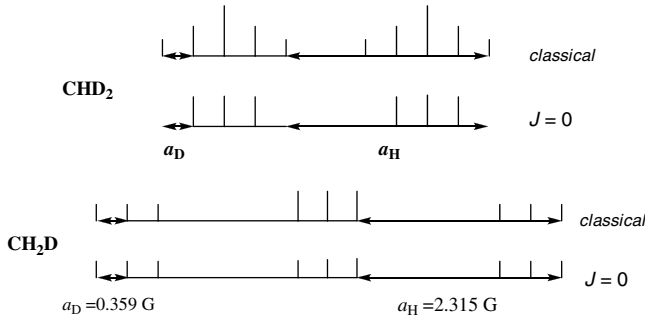

Figure 8. Basic EPR stick spectra for methyl-like, mixed-isotope proton–deuteron rotors indicating the quantum effects due to the ground rotational level. The corresponding experimental spectra at liquid He and higher temperatures are shown in figure 9.

$$\begin{aligned} \psi^{\mathrm{A}}_{-1} &= [|\bar{1}\ 0\rangle + |0\ \bar{1}\rangle]/\sqrt{2} \\ \psi^{\mathrm{A}}_{1} &= [|0\ 1\rangle + |1\ 0\rangle]/\sqrt{2} \\ \psi^{\mathrm{A}}_{0} &= [|1\ \bar{1}\rangle + |\bar{1}\ 1\rangle]/\sqrt{2}. \end{aligned} \tag{12b}$$

They comprise an approximate 1:1:2:1:1 deuteron hf pattern for the rotational $J = 1$ level and, when superimposed on the B lines of the ground rotational $J = 0$ level, they reach the fast rotation intensity distribution 1:2:3:2:1, because of the negligibly small second-order shifts. Similarly to the case of the CD_3 radical the $J = 1$ levels are easily populated as the temperature increases since their rotational energy is half in comparison to the proton radical. In fact, the spectrum reaches a classical appearance at the relatively low temperature of 10 K.

In a similar manner, in figure 9 the EPR spectrum of the isotope-mixed radical CH_2D is seen, consisting of a major proton triplet with equal intensity (of smaller deuteron triplets) which can be easily attributed to totally symmetric A nuclear spin states (in C_2) of two protons with $F = 1$.

Knight *et al* [30] have observed similar nuclear spin states for H_2O^+ radical cation isolated in an Ne matrix at low temperatures close to 4 K. In the higher temperature spectrum of CH_2D at 25 K the contribution of the first rotational level ($J = 1$) is visible, shifted by the second-order shift, see figure 9.

This short account of the mixed H-, D-methyl-like rotors does not exhaust the topic, which is also interesting due to the similarity of the above mixed rotor radicals to other important radicals such as NH_2, which have a magnetic central atom. They share the low C_2 symmetry required for quantum effects of the exchange of identical protons but can behave differently. A more thorough investigation is necessary in order to reveal further details.

3. Experimental part

3.1. Sample preparation and experimental set-up

The solid samples under study were obtained by gas condensation on the thin-walled bottom of a quartz finger filled with liquid helium at 1.5–4.2 K. The bottom of the finger, which served as a substrate where the major part of the matrix

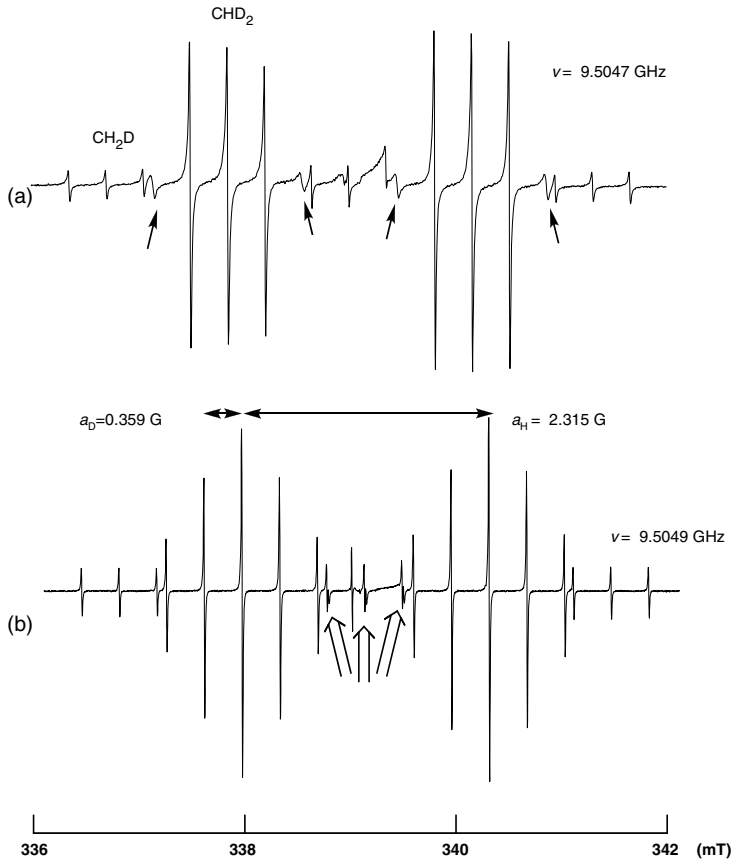

Figure 9. High-resolution EPR spectra of the CH_2D and CHD_2 radicals in Ar matrix at (a) 4.2 K and (b) 25.0 K, respectively, from [1]. Out of the wings of the strong triplets of CHD_2 at 4.2 K, belonging to the ground rotational level ($J = 0$), are seen the four weak transitions (single arrows) with relative intensity of approx. 10:1. They belong to the next rotational level ($J = 1$) and are fully developed at 25 K seen in (b). The double arrows in (b) indicate the contribution of the first rotational level ($J = 1$) to the central triplet of the CH_2D spectrum. They are high-field-shifted compared to the spectrum of the ground rotational level.

gases was condensed, was located at the center of the evacuated microwave cavity of the EPR spectrometer. figure 10 shows the major section of the experimental set-up: the microwave cavity of the 3 cm EPR spectrometer with 100 kHz modulation of the magnetic field, the low temperature gas discharge device and the quartz finger. Here 1 is the cylindrical TE_{011}-mode cavity, 2 is the bottom of the quartz finger 3, filled with liquid He, and 4 is a waveguide. An electrodeless RF gas discharge is excited in the glass tube 5 with outlet 6 of 0.6 mm diameter. The matrix gas can be supplied to substrate 2 by glass tube 7 and further by quartz tube 8 inserted into the cavity (channel B). The end of the tube 8 is located close (3 mm) to the bottom 2 which facilitates effective freezing out of the matrix gas. The whole device presented in the figure is cooled externally with liquid nitrogen vapor (LN_2) and its temperature can be varied from 77 to 300 K. A high-frequency (15 MHz) oscillator is used to maintain the discharge. The high-frequency power is fed through a coaxial cable to coil 9 wound over discharge tube 5. The oscillator can be operated either in pulse or continuous regime. The base pressure in the experimental chamber is 3×10^{-6} Torr. We used pure gases with the following impurity content: 0.004% Ne, 0.0009% Kr, 0.007% Ar, 1% CO (N_2 being a major impurity). The molecular hydrogen was purified via pressure-driven diffusion across a palladium membrane which was a heated palladium–silver metallic tube.

In Kr-matrix experiments, pure Kr was fed through channel **B**, while another Kr flow with a small admixture of CH_4 was supplied through channel **A**. The methane content varied in the gaseous mixture from 1% to 10% in different Kr experiments. In the discharge zone, CH_3 radicals formed through dissociation of CH_4 molecules.

The gas fluxes were measured by the consumption from store balloons. Taking into account the geometry of the deposition system, the whole CH_4 impurity content in the solid was estimated to vary from 0.15 % to 0.5%.

To give a hint about the thickness of the sample film, let us consider 90 cm^3 of Kr under normal conditions (about 0.004 mol) which was passed through channel **B** onto the substrate in a given run. It was mentioned above that the major part of the matrix gas flow condenses on the bottom (2) of the quartz finger. The bottom area is approximately 1 cm^2. Given the solid Kr density of 3090 kg m^{-3}, according to a paper by Pollack [31], the film thickness would be about 1 mm. This value may be considered as the upper limit of the thickness.

Based on this thickness assessment, some estimation of the temperature gradient across the film may be obtained. The solid Kr thermal conductivity is 0.6 W $(m\,K)^{-1}$ at 4 K according to Pollack's paper [31]. The major part of the thermal load of the substrate arises from thermal radiation. Let us consider the substrate covered by

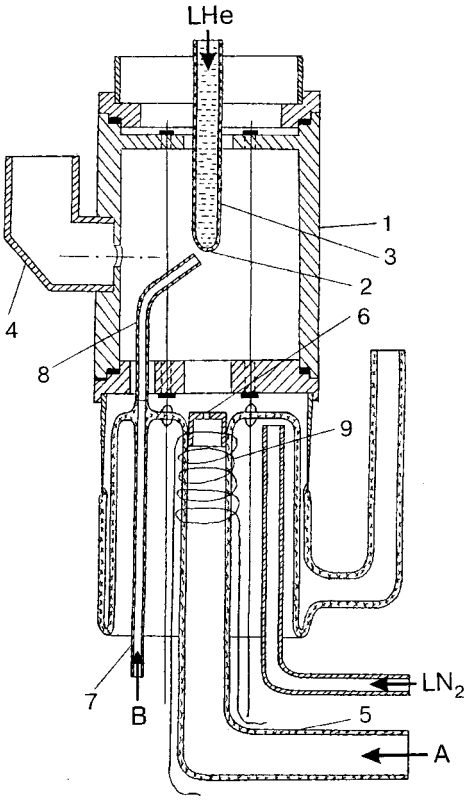

Figure 10. The main part of the experimental set-up including the microwave cavity of the EPR spectrometer, the gas discharge system, the gas inlet tube for matrix gas and the quartz finger cooled by liquid helium. For the explanation of the numbers see in the text.

condensed Kr film to be almost black body with emissivity $\varepsilon \approx 1$. The thermal radiation load for the condensation area with $\varepsilon = 0.9$ shielded by an 80 K baffle is 1.85×10^{-4} W cm^{-2} [32]. Then, the temperature gradient would be $\Delta T = 0.003$ K for the 1 mm thick film. Even if the above value presents the lower limit for ΔT, the temperature gradient, nevertheless, is only a minor fraction of 1 K.

3.2. The broadening problem

Comparing the low temperature EPR spectra of CH_3 radicals by Dmitriev with collaborators [11] to the spectra published by Benetis with the Japanese group [1], it is obvious that Dmitriev's spectra were always broader and possessed in general more classical characteristics. The extreme level of sharpness of the Japanese-group lineshapes becomes particularly obvious by the fact that even the sk^{13}C satellites for the methyl radical with natural carbon could be detected in the background of the spectra due to the favorable S/N conditions, see figure 2 in [1].

As an example of the correspondence between quantum and classical behavior we refer to the broadening from pure dipole–dipole interaction due to incomplete rotational averaging of the methyl radical. The dipolar part of the hyperfine interaction was shown to vanish in the ground level according to equation (8), but had a non-zero quantum average for higher levels [1]. The slightly different quantum averages of it for different rotational levels could probably appear as unresolved splitting when few higher rotation levels were occupied. The splitting was proportional to the small residual anisotropy $A_{\parallel} - A_{\perp}$ and finally appeared as a second-order shift for classical conditions of rotations at the highest experimental temperatures [1].

An example of the transition to classical behavior concerns the CF_3 radical. The approx. 19 times larger mass of the fluorine nucleus ^{19}F compared to the proton ^{1}H, leads according to equation (4) to about 32 times smaller rotational constant values for CF_3 compared to CH_3 (the covalent radii from the web periodic table [33]: carbon 77 pm; proton 37 pm; fluorine 71 pm were used). This gives approximately a separation of 0.18 K for the rotational states of fluorine-substituted methyl radicals. In such a case, the thermal energy even at liquid He temperatures CF_3 populates a large number of high rotational states, bringing the system to the 'classical' limit where the Boltzmann distribution is valid. In contrast, for CH_3 with almost 70 times greater rotation-level separation, quantum statistics are rather applicable.

This observation justifies the application of the free-quantum-rotor treatment of CH_3 at liquid He temperature, i.e. as the rotor which is not in appreciable contact with the lattice due to the limited thermal energy available [1]. Most importantly, under these conditions the methyl rotors can be considered as rotating free inside the structure of the solid host matrices [2]. This is generally possible for 'ultra-light' and 'highly symmetric' quantum rotors where interaction with the matrix is not large enough to quench rotation. The experimental EPR lineshapes are characteristically affected by this property. Even substitution of one of the protons by a deuteron does not alter certain fundamental properties of the rotor statistics as was discussed above.

It will be useful also to notice that radicals with heavier central atoms than ^{13}C, such as the SiH_3 radical for example, and with heavier peripheral atoms such as the CF_3, can obtain a pyramidal configuration [5, 34], resulting in a modified moment of inertia tensor. Due to the modified symmetry of the molecule, different matrix–rotor interactions will also be a consequence.

In fact, one should not be surprised that the obtained EPR spectrum of the pyramidal CF_3 radical in Kr, with the heavy peripheral fluorine atoms instead of protons or deuterons, was powder-like.

To start with, we mention two trivial possible causes of this difference: the sample preparation and instrumental set-ups and their respective deficiencies.

To the deficiencies of the sample preparation belongs, for example, a temperature gradient throughout the sample.

The variation of the broadening with the temperature gradient in the sample can be very significant depending on the temperature range in question, since the quantum and the classical conditions of the rotary motion are very narrow. As was mentioned in several places in this review a difference in temperature of about 10 K readily leads to classical characteristics of rotation of the spectra.

Furthermore a 'natural' source of broadening could be the presence of magnetic isotopes in certain matrices, e.g. in the Kr matrix, with a concomitant increased interaction of the matrix with the radical.

The above proposed potential sources of broadening, as well as instrumental parameters of the EPR signal, such as MW (microwave) saturation, are enumerated in the following and are evaluated against the conditions of sample preparation given at the beginning of section 3.

Deposition conditions. We should point out that, compared to radiolysis, the deposition method described above has the advantage that it can easily go down to 1.5 K, so that it could eliminate remnants of the CD_3 spectrum in figure 7 from the $J = 1$ rotational level.

(a) The experimental sample condensation on 'cold finger' might lead to a not uniform sample and may involve temperature gradients through the sample due to the asymmetry of the adsorption surface.
The estimations performed in the experimental part show that the temperature gradient in the sample is expected to be insignificant. The only exception is when the sample film is a non-equilibrium deposit and undergoes, occasionally, structural rearrangement followed by energy relaxation.

(b) For preparations of small thickness one should expect 'boundary surface effects' and even non-symmetric hindering potentials if the environment of the radicals in the sample is not homogeneous due to the closeness to the surface of different sections of the matrix.
According to the above sample preparation and experimental set-up, see figure 10, the film thickness obtained on the surface of the cold finger would be about 1 mm, consisting of a large enough number of molecular layers of the matrix molecules so that boundary effects were avoided.

(c) Stronger rotor–matrix interaction in matrices of larger, non-spherical and/or dipolar molecules leading equivalently to conditions of motion in the classical limit.
Some important aspects of this issue are examined in detail further for the case of the deposition of methyl in a Kr matrix.

Instrumental parameters. In general, for the methyl-radical spectra in inert gas matrices one has to consider all the conditions for the CW spectrum acquisition from first principles.

For example, we reproduce in this work the effects of saturation that were observed in Dmitriev's most recent work concerning EPR spectra of methyl radicals in quench-condensed krypton films [4]. At sufficiently large MW power, the two central narrow lines split so that the narrow-line series takes an appearance recorded elsewhere for CH_3 in Ar at higher temperatures above 12 K. Simultaneously, the intensity of two central broad lines increases dramatically while the outer components saturate.

(a) *MW-power saturation.* The methyl rotor spectra obtained in an Ar matrix by the Japanese group [1] at liquid He temperatures of about 5 K were exceptionally sharp and therefore were extremely sensitive to saturation by MW power. At least half of the broadening is equal to the inverse spin–lattice relaxation time T_1 (lifetime broadening) which is very long at very low temperatures, explaining partially the unusual sharpness. The EPR spectra of the CH_3 radical at very low temperatures were thus easily saturated.
Regularly, saturation broadens the EPR lines and therefore saturation was kept at the lowest possible level in the experiments of the Japanese group. In the present work several tests with variable MW power and temperature conditions were performed, aiming at the illumination of the saturation effects.

(b) *Modulation frequency during the CW acquisition.* It is known that magnetic field modulation may also cause line broadening. The broadening is considered to be negligible if the modulation frequency, f_m, is much smaller than the linewidth [35]; the relation

$$f_m \ll (\gamma/2\pi) \cdot \Delta H, \qquad \text{where } \gamma = 2\pi g\beta/h \quad (13)$$

should thus be valid. Considering the values of the natural constants used (the relation between Hz and G) the above expression may be written in a practical way as $f_m/\Delta H \ll 2.8 \times 10^6$ Hz G^{-1}. For a line of $\Delta H = 0.15$ G width and the modulation frequency of 100 kHz, like that used in Dmitriev's experiments [26], one obtains: $f_m/\Delta H = 0.7 \times 10^6$ Hz $G^{-1} \approx 0.238 < 1$. Hence, the frequency modulation could contribute somewhat to the linewidth. As for the amplitude of the modulation, this was kept as small as 0.04 G and, therefore, suggested almost no contribution to the linewidth.

3.3. Matrix deposition effects

In Benetis' studies with the Japanese group certain quantum mechanical reasons are also found for that very small broadening [1]. The quantum properties which give sharp EPR lineshapes were observed in planar CH_3 and CD_3 radicals in Ar. At 4–5 K, instead of the powder spectrum expected by considering the hyperfine coupling of the three alpha-protons (6.5 times smaller for D), the experimental transitions obtained were sharp and isotropic.

The variable broadening in the transitions of the lowest level quartet obtained by Dmitriev and Zhitnikov [11] was attributed to the simultaneous anisotropy of both the **g** tensor and the hfi **A** tensor. In particular an M_F-dependent broadening of the $|FM_F\rangle$ multiplet [36] given by

$$\Delta H = a + bM_F + cM_F^2 \quad (14)$$

agreed rather well with the experimental spectra in that work.

The broadening ΔH was visible also as the normally observed inversely related apparent intensity of the sharp experimental transitions in the spectra of all systems studied. This is similar to the originally classical differential broadening due to relaxation through the cross correlation of simultaneously active **g** and **A** tensor anisotropy. The peculiarity here is that the latter is due to the coupling of the spins to a classical lattice and requires rather slow modulation of the tensors by rotational diffusion, not inertial rotation. In contrast, for temperatures close to 4 K, the system can be

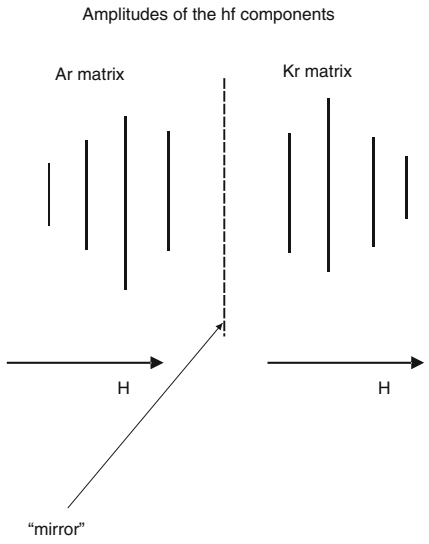

Figure 11. The amplitude sequence in the EPR quartet of the ground rotational level of the CH_3 radical in cryogenic Kr matrix is a mirror image of that in Ne, Ar, N_2 and CO matrices.

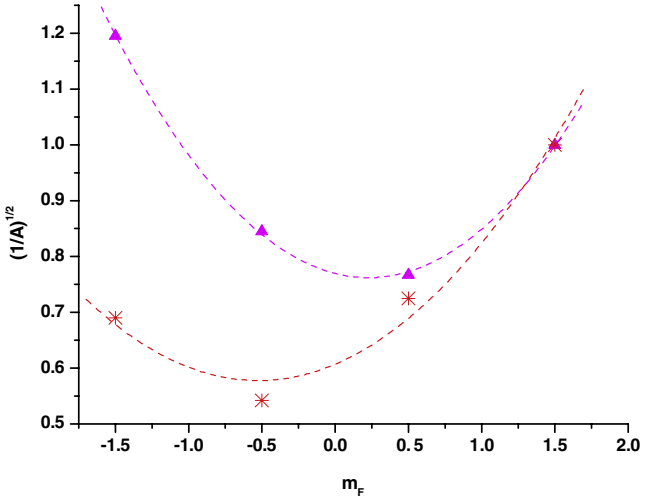

Figure 12. Variation of the inverse square root amplitude with the total nuclear spin projection M_F of the EPR transitions of CH_3 radicals trapped in very cold matrices; ∗—Ar matrix; ▲—Kr matrix.

considered as isolated, while diffusion requires good contact with the lattice.

Another striking observation is that the amplitude sequence of the EPR spectrum of CH_3 in Kr is a mirror image of the CH_3 spectrum in practically all the other matrices, Ne, Ar, N_2 and CO, as seen in figure 11 which displays a rough sketch of the phenomenon. In our experimental spectra, going from the low-field to the high-field component, the amplitude sequence is 1:1.9:3.4:2.1 for the CH_3 in Ar [26] and 1:1.7:1.4:0.7 for the CH_3 in Kr [4]. This discrepancy can be interpreted by a change of the sign of the coefficient b in the linear term of the above binomial in M_F of equation (14). The change of the sign is possible irrespective of the sign of the hf coupling because the coefficient b corresponds to the cross relaxation of the Zeeman and the dipolar interaction, being proportional to $(g_\parallel - g_\perp) \cdot (A_\parallel - A_\perp)$. In particular the coefficients b and c have the same signs for Ar and opposite signs for Kr.

The present results substantiate earlier findings [11]. Possible explanations have also been presented in [26] and are supported also by table 3 which lists the spacing between hf components in the Ar and Kr matrices. The data in table 3 clearly show a matrix effect resulting in decreased hf spacing for CH_3 in Kr compared to CH_3 in Ar. This spacing increases from the low-field to the high-field component, an effect that was attributed to the second-order correction to the line position [1].

The anisotropies found for CH_3 in Ar and Kr are compared in figure 12, while the difference in the overall spectral appearance was shown in figure 11. In figure 12 the value of $A^{-1/2}$ is plotted against the total nuclear spin projection, M_F, A being the amplitude of the corresponding hf component and the inverse square root of the amplitude, $A^{-1/2}$, is proportional to the component's width ΔH. This is based on the fact that $A \cdot \Delta H^2 \approx$ const, which is proportional, approximately, to the number of radicals, justifying the proportionality $\Delta H \sim A^{-1/2}$. This relation allows the fitting of the experimental dependences with the function in equation (14). Dashed curves in figure 12 show the results of the fitting procedure.

Table 3. The spacing between neighboring hyperfine components for the CH_3 radical trapped in Kr and Ar matrices.

	Component numbers and spacing in Gauss			
Matrix	I–II	II–III	III–IV	Reference
Kr	22.87(4)	22.97(4)	23.19(4)	The present study
Ar	23.00(4)	23.12(4)	23.30(4)	[26]
Ar	23.00	23.15	23.30	[1]

Table 4. The values of the coefficients a, b and c of equation (14) determined by fitting experimental data in figure 12.

Matrix/coefficient	a	b	c
Ar	0.607 06	0.1113	0.105 75
Kr	0.769 56	−0.0663	0.145 75

These curves match fairly well the experimental amplitudes. Actually the two quadratic functions with minima to the left and to the right of $M_F = 0$ give an immediate perception about different signs of b in two cases. The values of the coefficients a, b and c are listed in table 4.

3.4. The Kr–CH_3 system

The experimental procedure and set-up used in the present study were described in detail above and in [37]. Briefly, a sample of matrix gas (solid Kr) doped with methyl radicals was formed on the low temperature surface of a quartz finger inserted into the microwave cavity. The sample temperature could be lowered down to about 1.5 K by pumping the vapor from the helium bath of the cryostat. The temperature was estimated by vapor pressure.

Normally, two gas flows were used. In the present study, the first one was gaseous Kr with a small admixture of CH_4.

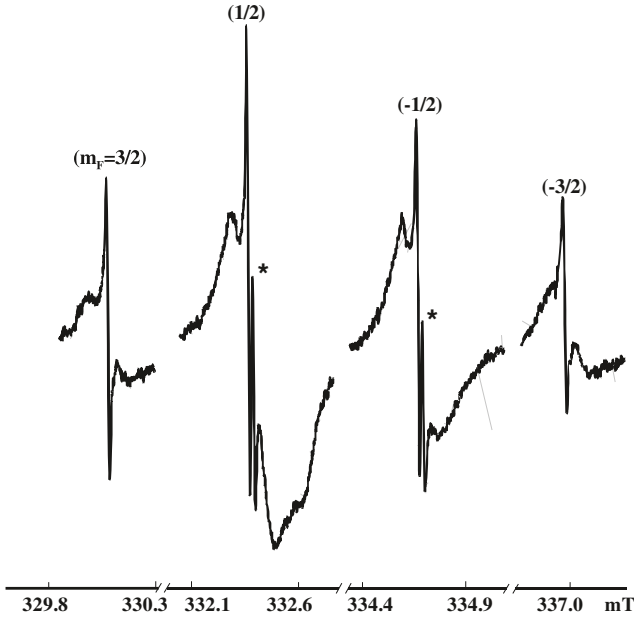

Figure 13. The 4.2 K EPR spectrum of methyl radicals trapped in solid krypton. Resonance frequency: $f_{res} = 9344.22$ MHz. The attenuation of the microwave power was 26 dB, obtained by using MW power, P, of about 40 μW and amplitude of the resonant MW field, B_1, of approximately 9 μT. The narrow lines of the 'E' symmetry doublet are marked by stars. The projection M_F corresponds to the F_z component of the total nuclear spin [4].

Prior to condensation, this flow passed through an electrodeless high-frequency discharge zone where CH_3 radicals formed through dissociation of CH_4 molecules. The second flow was extremely pure Kr that was fed onto the substrate avoiding the discharge zone.

3.4.1. Saturation. The gas fluxes were measured by the consumption from store balloons. Taking into account the geometry of the deposition system, the whole CH_4 impurity content in the solid was estimated to vary from 0.15% to 0.5%. The magnetic field of the spectrometer was modulated at 100 kHz. The base pressure in the experimental chamber prior to condensation was 3×10^{-6} Torr (see above about the details of the experimental conditions).

It was found out earlier [11] that the EPR spectrum of CH_3 in a Kr matrix at 4.2 K showed anisotropy in both the electron Zeeman (**g** tensor) and the hf interaction. The samples were deposited from the gas phase onto a cold substrate. The anisotropy revealed itself by the obtained asymmetric spectrum with different amplitudes and widths in the different hf components. The same spectra seen in figure 13 were obtained in the present study. Figure 14 shows the data on amplitudes, widths and intensities of the hyperfine components.

The amplitudes and widths are defined as the distances along the relevant intensity axes and resonant field, respectively, between the extrema of the derivative. The amplitudes are normalized to the first ($M_F = 3/2$) line amplitude. The projections M_F correspond to the z component of the total

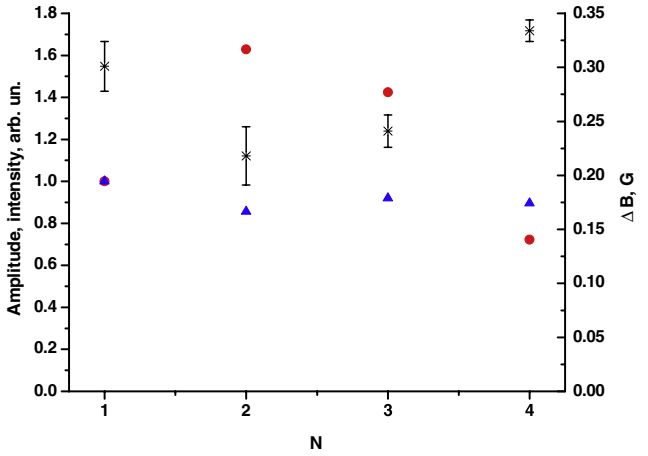

Figure 14. Amplitudes, widths and intensities of the hyperfine components of the ground rotational A-quartet of the CH_3 EPR spectrum in Kr. Here N stands for the line number going from low to high magnetic fields, $M_I = 3/2$ to $-3/2$ nuclear spin projections, respectively. The symbols in the figure correspond to, ∗—linewidth, ▲—intensity, ●—amplitude. The spectrum was recorded at temperature $T_{rec} = 4.2$ K.

Table 5. The parameters of the fitting procedure for the data in figure 15.

	Parameters			
HF component	P_1	P_2	P_3	P_{max}
I	329.558 03	0.264 52	0.703 2	0.651
II	276.581 25	0.269 07	0.680 38	0.746
III	453.531 82	0.283 74	0.720 38	0.644
IV	224.796 33	0.299 92	0.735 23	0.638

nuclear spin. The line intensities of the absorption derivatives are taken as the amplitudes multiplied by the widths squared.

It is seen in figure 14 that all intensities are nearly equal. This finding suggests that the quartet is due to the lowest rotational level of A symmetry [13, 38].

Further, the three-parameter expression:

$$A = \frac{P_1 P^{1/2}}{(1 + P/P_2)^{P_3}} \tag{15}$$

adapted here from [39] was used to fit the experimental data in figures 15 and 16.

By this expression the narrow A-lines were fitted rather well as seen from these figures.

At first glance, however, the formula does not work with E-lines.

Here, P is the microwave power measured experimentally, and P_1, P_2 and P_3 are adjustable parameters given in tables 5 and 6.

Outlining the physical meaning of the parameters: P_1 deals with the overall amplitude of a line while P_2 deals with the value of the MW power P at which saturation becomes significant. The value of P_3 increases with increasing 'rate' with which the saturation proceeds after the maximum of the saturation curve.

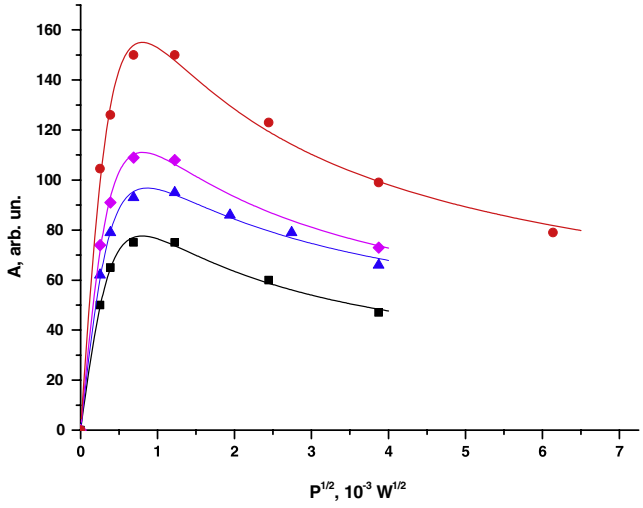

Figure 15. Saturation curves for the A-line hyperfine components of the CH_3 radical trapped in solid Kr. $T_{rec} = 4.2$ K. Components: ♦—first, ▲—second, ●—third, ■—fourth. In this figure no care is paid to the amplitude ratios of components, which are, therefore, arbitrary.

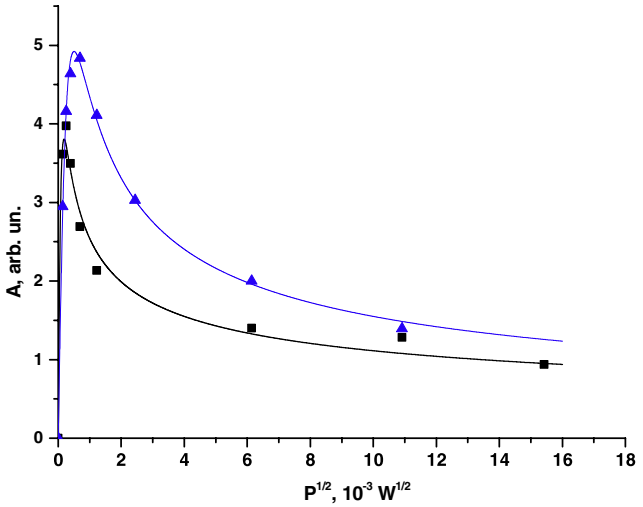

Figure 16. Saturation curves for the third component taken at two different temperatures: ▲—$T_{rec} = 4.2$ K, ■—$T_{rec} = 1.9$ K. For the functions and the parameters that fitted the experimental points see in the text and table 6.

The derivative of equation (15) was further computed and was set to zero, leading to the following value of the saturation power:

$$P_{max} = \frac{P_2}{2\,P_3 - 1}. \qquad (16)$$

The experimental data were taken at microwave powers low enough to ensure that the conditions were well apart from the saturation of the lines. It is shown from figure 15 that all four components saturate maximally at the same MW power. The spin–lattice relaxation time, T_1, was found to depend on the sample temperature, increasing with decreasing temperature, as seen in figure 16.

This temperature trend of T_1 for A-lines is in accordance with findings reported for CH_3–Ar deposition experiments at

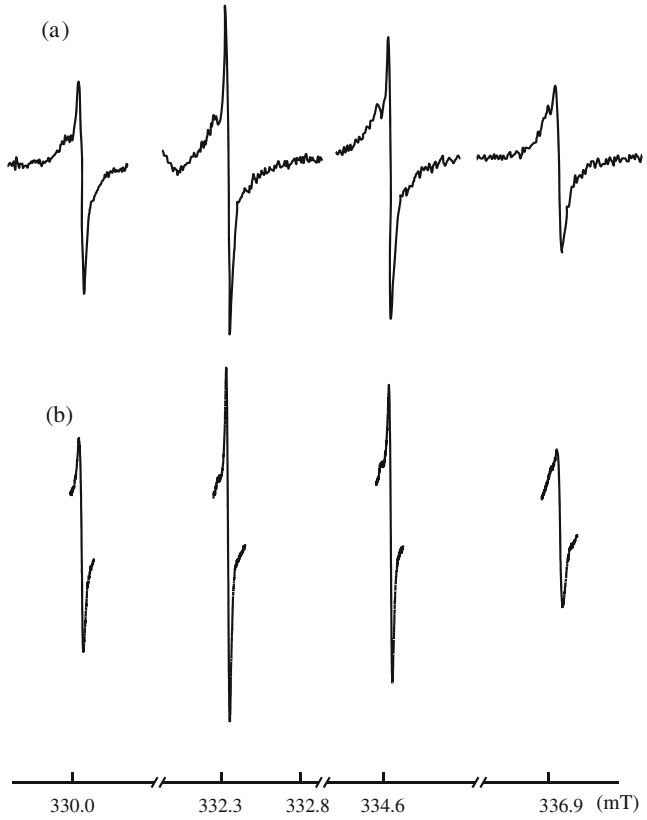

Figure 17. EPR spectra of CH_3 radical in Kr matrix. The substrate temperature during deposition was $T_{dep} = 4.2$ K. The microwave resonance frequency was $f_{res} = 9343.60$ MHz. The sample temperature during recording of the spectrum, T_{rec}, was (a) 4.2 K and (b) 2 K. The figure demonstrates that the extent of the anisotropy does not depend on the recording temperature T_{rec} of the spectrum.

Table 6. The parameters of the fitting procedure for the data in figure 16 and the computed values of the power P_{max} where the saturation curve has a maximum.

	Parameters			
Temperature (K)	P_1	P_2	P_3	P_{max}
1.9	49.926 52	0.012 79	0.681 17	3.53×10^{-2}
4.2	22.384 12	0.123 49	0.742 41	2.55×10^{-1}

temperatures above 14 K [5]. We have also found out that the sample temperature during recording the spectrum, T_{rec}, had either no, or negligible, effect on the extent of the anisotropy, figure 17.

On the other hand, the anisotropy of the CH_3–Ar spectrum was recently found to be smeared out with increasing temperature in the region above 14 K according [5]. Perhaps, one could observe the same effect in the case of the Kr matrix at much higher temperatures compared to those used in the present study. This temperature dependence may be explained both as owing to the dominance of the stochastic reorientation of the C_3 axis and also to the onset of the molecular reorientation about C_2 axes with rising temperature [4, 26, 10].

The effect had been either expected [10, 26] or observed [5] for matrices of spherical particles: Ne [10, 26], Ar [5, 10, 26] and Kr [10, 26]. On the other hand, for matrices

of the linear molecules, CO, CO_2 and N_2, a picture of the spectrum transformations with changing temperature is not certain.

It is expected [10] that the radical motion in these matrices would be governed by the motion of the matrix molecules, so that the EPR spectrum would be anisotropic for rising temperature, until the radicals disappear through the recombination process. Possibly, the EPR spectrum would start to become less asymmetric in the close vicinity of the annealing temperature of the matrix.

Although the substrate temperature during deposition, T_{dep}, has a noticeable effect on the spectrum anisotropy of the H atom in solid Kr in the temperature range of 1.5–4.2 K [40], we have not observed this effect for the CH_3–Kr system. This means that different mechanisms are underlying the appearance of the anisotropy for H compared to CH_3. Indeed, the extent of the anisotropy is nearly the same for the CH_3–Ar system at liquid He temperatures [26] as at 14 K [5].

Very interestingly, high-resolution EPR spectra of CH_3 achieved by X-radiolysis of the Ar matrix containing 0.2 mol% CH_4 showed no sign of anisotropy [1]. This is also obvious in figures 6, 7 and 9 that are reproduced in the present work.

The different concentrations of the CH_4 matrix impurity in the samples of the different research groups should not affect the observed differences. Indeed, we have found no change in the pattern of the spectrum in samples with different CH_4 concentrations either in Ar or Kr matrices. Moreover, the authors of [5] reported that their method was insensitive to the methane/argon ratio. They also carried out experiments with small impurity content: less than 0.03 mol% CH_4 in Ar. One may suppose that the difference in the anisotropy lies in the sample quality: quench-condensed films[8] in the present study and [10, 11, 26] compared to the solids with, probably, lower concentrations of imperfections [1]. Again, recent observations [5] suggest that this would not be the origin of the different findings on the spectrum anisotropy.

4. Discussion

In [1], the authors used a slow gas deposition method followed by radiolysis, which resulted in rather homogeneous samples and, to further minimize inhomogeneities, they carefully annealed the samples of the CH_3 radical in Ar at 30 K before spectral measurements. It seems now that the reason for the different results is due to different techniques of sample preparation: deposition in the present study by Dmitriev as well as in [5, 10, 11, 26] and radiolysis in [1]. As a result, the trapped radicals perform hindered rotation in the samples of the present work, while they are able to rotate freely in the case of radiolysis preparation.

To explain briefly the difference, when a CH_4 molecule in the cryogenic inert gas matrix absorbs a photon during radiolysis, it moves to an electronically excited state. After that, dissociation takes place with the release of an H atom and energy. An electronically excited molecule is able to distort the matrix cage, pushing atoms outwards. If the distortion is partly inelastic, the impurity molecules become 'more free' to rotate. Indeed, the effect of the cage distortion under electronic excitation was found in solid rare gases, see e.g. [41] and references therein. Interesting research which is relevant to the present discussion was also published earlier, [42]. In that work, NO impurity in Ne was excited inducing a rearrangement of the surrounding medium. The authors consider this as a model for the pure noble gases where the rearrangement was found to be not completely elastic.

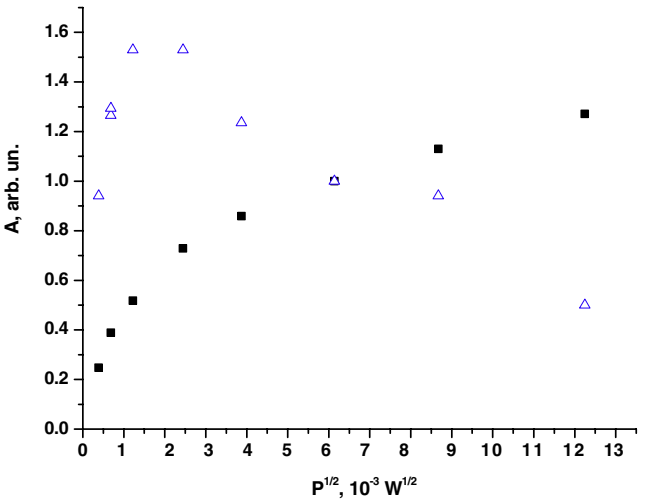

Figure 18. Saturation behavior for two of the 'broader' lines of the EPR spectrum of the CH_3 radical in a Kr matrix shown in figure 13; △—first component, ■—third component. The spectrum was obtained at temperature $T_{rec} = 4.2$ K.

Concluding, it seems that neither CH_4 impurity nor imperfections of the structure of the solid matrix affect the spectral asymmetry. Annealing could not be a reason either because in the study by Popov *et al* [5] the samples were annealed at 30 K before spectrum measurements. Hence, the most probable reason is the difference in the sample preparation techniques.

Actually no matrix is really inert. Thus, considering that the matrix plays an important role for the sample preparation, further research is required to resolve this problem, maybe including the formation, the deposition of the matrix and the interaction of the radicals with the matrix molecules.

A striking result has been obtained very recently for the CH_3–Kr system [4]. Two additional sets of EPR lines for trapped CH_3 radicals have been obtained: four additional broad and two narrow components with peak-to-peak linewidths $\Delta B \approx 1.8$ G and $\Delta B \approx 0.2$ G, respectively. At low microwave power in the cavity the broad components are of nearly equal intensity. The two additional narrow lines are high-field-shifted by 0.245(25) G compared to the central narrow A-lines, thus occupying exactly the expected E-line position [1, 5]. These lines are observable only at high microwave powers when the narrow A-lines are saturated. Interestingly, the two outer broad components saturate more rapidly than the two inner broad components, figure 18. In their saturation behavior, the outer broad lines resemble the

[8] Quench-condensed gas films are systems far away from thermodynamical equilibrium. These systems are obtained through growing the films by vapor deposition of atoms onto a substrate held far below their melting point.

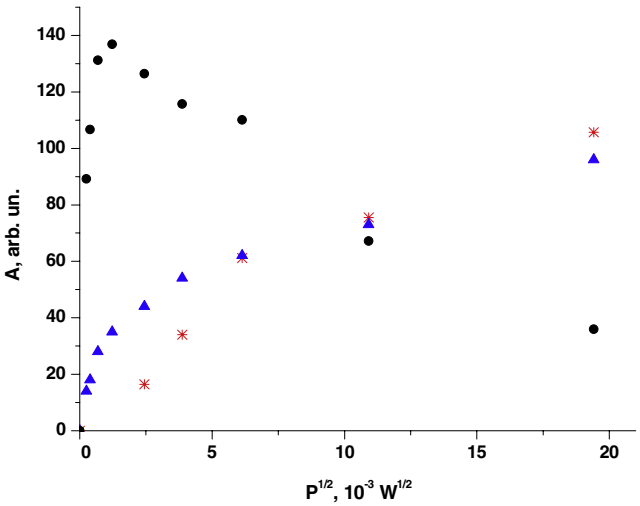

Figure 19. Saturation behavior of the three overlapping transitions which comprise the third hf component recorded at temperature $T_{\rm rec} = 4.2$ K. ●—the narrow 'A'-line; ▲—the broad line; ∗—the narrow E-line.

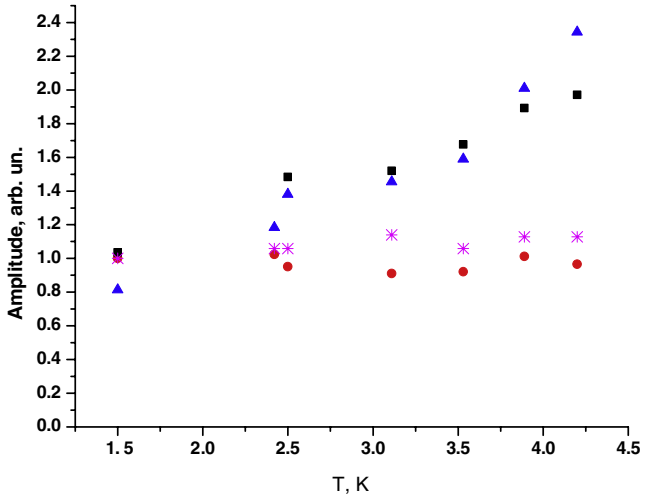

Figure 20. Amplitudes of all the different lines comprising the third hf component plotted against the sample temperature. ●—the narrow 'E'-line taken at 26 dB attenuation of the microwave power with $P \approx 40$ μW and $B_1 \approx 9$ μT; ■—the narrow A-line taken at 26 dB; ▲—the broad line taken at 26 dB; ∗—the narrow A-line taken at 53.7 dB with $P \approx 65$ nW and $B_1 \approx 0.6$ μT.

narrow A-lines, while the inner broad lines saturate rather like two narrow 'E'-lines. This is also seen from figure 19.

An explanation for this latter characteristic, which is related to the different couplings of the lattice with the $J = 0$ and 1 rotational level, is attempted further.

The spectrum of the broad lines is supposed to consist of four A-lines of equal intensities and two E-lines. The central lines appear to be broader by the overlap of the A- and E-lines discussed above. As the MW increases the sharper A-lines saturate more rapidly, leaving behind a larger proportion of the E-lines. It is therefore the central lines that contain also the E contribution that prevails for higher MW power.

The sample temperature affects not only the spin–lattice relaxation time, T_1, of the narrow A-lines, figure 16, but the T_1 of the broad lines as well, whose value is increased with lowering the temperature. On the other hand, the same conclusion is not obvious for the narrow 'E'-lines. Figure 20 shows the dependence of the amplitudes on the sample temperature. At large microwave power, the amplitudes of both the broad and the narrow A-lines decrease with decreasing temperature, an effect which is, to a large extent, due to the saturation being more prominent at low temperatures. Indeed, the amplitude of the A-line taken at low microwave power shows almost no sensitivity to the sample temperature variation.

The same observation holds for the narrow 'E'-lines. Thus, the properties of the 'E'-lines do not depend on the sample temperature. This result is expected from the discussion and the experimental data presented earlier [4]. On the other hand, the E-lines observed in the EPR spectrum of CH_3 in Ar [1, 5] showed not only strong temperature dependence of the amplitude, but also of the width, i.e. the lines became weaker and broader with decreasing temperature.

Let us consider that the magnitude of the energy difference between $J = 0$ and 1 rotational levels of CH_3 in Kr, $\tilde{\varepsilon}_{1\pm1,M}$, is close to that of CH_3 in Ar, $\Delta E = 16$ K [5]. The ratio of corresponding populations for the A-state, $P_{\rm A}$, and the E-state, $P_{\rm E}$, at a given temperature may be computed by the following expression [5]:

$$\ln\left(\frac{P_{\rm A}}{P_{\rm E}}\right) = \ln\left(\frac{{\rm e}^{-\varepsilon_{000}/k_BT}}{6\,{\rm e}^{-\varepsilon_{1\pm1,M}/k_BT}}\right) = \tilde{\varepsilon}_{1\pm1,M}\frac{1}{T} - \ln(6). \quad (17)$$

Therefore, the ratio of $P_{\rm E}$ populations at 1.5 and 4.2 K would be

$$\frac{P_{\rm E}(1.5)}{P_{\rm E}(4.2)} = \exp\left[-\tilde{\varepsilon}_{1\pm1M}\cdot\left(\frac{1}{1.5}-\frac{1}{4.2}\right)\right] = 1.01\times10^{-3}. \quad (18)$$

On the other hand, the EPR signal intensity increases with decreasing temperature [35]:

$$Y_{\rm D} = Y_0\frac{1-\exp(-h\nu/kT)}{1+\exp(-h\nu/kT)} \quad (19)$$

where Y_0 is the signal intensity at $T \to 0$. Then

$$\frac{Y_{\rm D}(1.5)}{Y_{\rm D}(4.2)} = 2.78. \quad (20)$$

Taking into account equations (17) and (20), one comes to the conclusion that the E-line would constitute at 1.5 K only about 0.3% of its value at 4.2 K.

Thus, two questions are to be answered in the present study: first—the fact that E-lines are observed at very low temperatures down to 1.5 K; and second—the difference in the E-line transformations with temperature in the present study and [5]. We suppose that the present investigation concerning the temperature dependence of the saturation behavior substantiates the following explanation about the nature of the observed lines as was discussed in [4].

It was suggested there that the overlapping narrow-line series originated from the EPR spectra of CH_3 radicals trapped

in two different matrix surroundings. One indication for that is the existence of the substitutional position with cubic symmetry in the non-distorted fcc (face centered cubic) Kr crystal lattice which gives no observable E-lines at liquid helium temperatures. Another indication is the existence of a regular position with axial symmetry in the lattice which yields both 'A-lines' and 'E-lines' at low temperatures, provided that the difference of the rotational levels ΔE for CH_3 in Kr is small enough, allowing the admixture of higher and lower rotational levels. Probably the hosts of this kind are the hcp (hexagonal close-packed) crystallites which may form in the quench-condensed Kr. The evidence for hcp formation in quench-condensed gases, including Kr solid, was published earlier by various research groups [43, 44].

Pulsed NMR used to study ortho-H_2 as a dilute impurity in solid gases revealed axial sites for H_2 in Kr. As for the CH_3 broad lines they come from radicals in disordered regions of low symmetry.

Again, because of their low symmetry, the 'E'-lines merge at sufficiently high microwave power and overlap with the broad A-lines; these two different kinds of lines are not totally resolved and separable from the narrow ones. The fact that the intensity ratios of the A and 'E' to the broad lines vary substantially from one run to another supports the above suggestion.

5. Conclusions

The EPR spectra of the methyl rotor CH_3 and partially or fully deuteron-substituted variants CH_2D, CHD_2 and CD_3 in the temperature range 1.5–25 K display unusual features, such as extreme sharpness and exclusion of certain EPR transitions. The methyl radical was found to be planar already from early theoretical and experimental work [45], a fact that was never seriously questioned in more recent work to our knowledge. We have assumed the same geometry in all the above-mentioned partially and totally deuterated variants.

The main explanation for the sharpness of the EPR spectra of methyl-type rotors in an Ar solid at cryogenic temperatures is that the anisotropy of both the electronic Zeeman and the hyperfine interaction have trivial quantum averages for the ground rotational level. In particular the anisotropy of the hyperfine interaction averages to zero by rotation even in the higher rotational levels. The inertial free rotation of the light rotors with relatively high D_3 symmetry and the exchange symmetry of the identical protons or deuterons of the radical was the reason for the exclusion of certain EPR transitions. The EPR spectra of these radicals in an Ar matrix were noticeably affected by these properties and even in the spectra of the less symmetric mixed CHD_2 and CDH_2 rotors, clear quantum effects, mainly intensity distribution anomalies, were observed. The above cases are clearly different from the case of the CF_3 radical which, due to the large moment of inertia, possesses the expected classical broad line features and regular intensities of the expected transitions.

In more recent EPR experiments, it was shown that the anisotropy of the orientationally disordered CH_3 samples in frozen gases obtained by deposition on a glass substrate was larger than in earlier solid Ar samples obtained by radiolysis of deposited methane.

This anisotropy was, however, insignificant compared to the classically expected powders and was limited to asymmetric lines and extra line splitting. The stronger van der Waals interaction between the methyl radicals and the less inert matrix molecules, like Kr, N_2 and CO as compared to Ar, the dipole–dipole interactions (N_2 and H_2) or the possibility of smaller empty space (Ne) can be some of the possible reasons.

Also, given the slow o- to p-transition of the liquid He temperature hydrogen molecule matrix, the effects of the superhyperfine coupling of the magnetic active o-state on the broadening were also discussed. Differential saturation of the A-and E-lines of different symmetry were also observed experimentally.

The effects of differences due to sample preparation, due to MW power saturation conditions during spectral acquisition, and due to the matrix composition, were also discussed as they can be the reason of the extra broadening compared to the CH_3 samples in Ar prepared by radiolysis. It was shown that neither sample quality (the density of structure faults) nor CH_4 impurity concentration in the solid was responsible for the EPR spectral anisotropy. Hence, the most probable reason is the difference in the sample preparation techniques.

Acknowledgments

NPB acknowledges the support for the fulfilment of this work by the Director of the Technological Educational Institution, TEI of West Macedonia Dr George Charalampidis. Also support is acknowledged from the Russian Foundation for Basic Research under grant 08-02-90409-Ukr_a.

References

[1] Yamada T, Komaguchi K, Shiotani M, Benetis N P and Sørnes A R 1999 High resolution EPR and quantum effects on CH_3, CH_2D, CHD_2 and CD_3 radicals under argon-matrix isolation conditions *J. Phys. Chem.* A **103** 4823–9

[2] Press W 1981 Single-particle rotations in molecular crystals *Springer Tracts in Molecular Physics* vol 92 (Berlin: Springer)

[3] Sørnes A R, Benetis N P, Erickson R, Mahgoub A, Eberson L and Lund A 1997 Effect of isotopic substitution on the electron spin dynamics of the $CH_3C^{\bullet}(COOH)_2$ radical in x-irradiated methyl malonic acid powder: intrinsic potentials and activation energies *J. Phys. Chem.* A **101** 8987–94

[4] Dmitriev Yu A 2008 Peculiarities of EPR spectra of methyl radicals in quench-condensed krypton films *Low Temp. Phys.* **34** 75–7

[5] Popov E, Kiljunen T, Kunttu H and Eloranta J 2007 Rotation of methyl radicals in solid argon matrix *J. Chem. Phys.* **126** 134504

[6] Barbon A, Brustolon M, Maniero A L, Romanelli M and Brunel L-C 1999 Dynamics and spin relaxation of tempone in a host crystal. An ENDOR, high field EPR and electron spin echo study *Phys. Chem. Chem. Phys.* **1** 4015–23

[7] Goeffroy M, Kispert L D and Hwang J S 1979 An ESR, ENDOR, and ELDOR study of tunneling rotation of a hindered methyl group in x-irradiated 2,2,5-trimethyl-1,3-dioxane-4,6-dione crystal *J. Chem. Phys.* **70** 4238–42

[8] Bonon A, Brustolon M, Maniero A L and Segre U 1992 An ENDOR study of the temperature dependence of methyl tunnelling *Chem. Phys.* **161** 257–63

[9] Lindgren M, Eaton G R, Eaton S S, Jonsson B-H, Hammarström P, Svensson M and Carlsson U 1997 Electron spin echo decay at a probe of aminoxyl environment in spin-labeled mutants of carbonic anhydrase *J. Chem. Soc. Perkin Trans.* **2** 2549–54
Zecevic A, Eaton G R, Eaton S S and Lindgren M 1998 Dephasing of electron spin echoes for nitroxyl radicals in glassy solvents by non-methyl and methyl protons. *Mol. Phys.* **95** 1255–63

[10] Dmitriev Yu A 2005 EPR of matrix isolated methyl radicals *J. Low Temp. Phys.* **139** 541

[11] Dmitriev Yu A and Zhitnikov R A 2001 EPR study of methyl radicals. Anisotropy and tumbling motion in low-temperature matrices *J. Low Temp. Phys.* **122** 163

[12] Dmitriev Yu A and Benetis N P 2009 in preparation

[13] Freed J H 1965 Quantum effects of methyl-group rotations in magnetic resonance: ESR splitting and linewidths *J. Chem. Phys.* **43** 1710

[14] Sørnes A R and Benetis N P 1998 The EPR spectrum of the general $>C^{\bullet}–CX_3$ quantum rotor *Chem. Phys.* **226** 51–170
Sørnes A R and Benetis N P 1998 Theory of ESEEM in isotropic tunneling methyl rotor systems *Chem. Phys. Lett.* **287** 590–6

[15] Apaydin F and Clough S 1968 Nuclear magnetic resonance line shapes of methyl groups undergoing tunnelling rotation *J. Phys. C: Solid State Phys.* **1** 932

[16] Mottley C, Kispert L D and Clough S 1975 Electron–electron double resonance study of coherent and random rotational motion of methyl groups *J. Chem. Phys.* **63** 4405–11

[17] Owen N L 1974 *Internal Rotation in Molecules* ed W J Orville-Thomas (New York: Wiley) chapter 6

[18] Clough S and Poldy F 1973 Tunneling rotation of a deuterated methyl group *J. Phys. C: Solid State Phys.* **6** 2357

[19] Sørnes A R and Benetis N P 1997 The methyl-rotor electron-spin dynamics in the Smoluchowsky drift-diffusional model framework *J. Magn. Reson.* **125** 52–64

[20] Erickson R, Nord U, Benetis N P and Lund A 1992 ESR lineshapes and methyl rotation in the acetic acid anion radical *Chem. Phys.* **168** 91–8

[21] Benetis N P, Mahgoub A S, Lund A and Nordh U E 1994 Rotation of deuterated methylene groups in the diffusional regime. Isotope effect of anisotropic alpha-Deuterons on ESR lineshapes of $^{\cdot}CD_2–COO^-$ radical in irradiated ZnAC dihydrate single crystal *Chem. Phys. Lett.* **218** 551–6

[22] Shiotani M, Yamada T, Komaguchi K, Benetis N P, Lund A and Sørnes A R 1998 The meeting on tunneling reactions and low temperature chemistry *JAERI-Conf. 98-014* pp 58–63

[23] Zare R N 1988 Angular momentum *Understanding Spatial Aspects in Chemistry and Physics* (New York: Wiley)

[24] Carrington A and MacLachlan A D 1967 *Introduction to Magnetic Resonance with Applications to Chemistry and Physical Chemistry* (New York: Harper and Row)

[25] Kubota S, Iwaizumi M, Ikegami Y and Simokoshi K 1979 Anisotropic hyperfine interaction in the electron spin resonance spectrum of the methyl radical trapped in $CH_3COONa{\cdot}3D_2O$ crystal at low temperatures *J. Chem. Phys.* **71** 4771

[26] Dmitriev Yu A 2004 High resolution EPR and the origin of the spectrum anisotropy of CH_3 radicals in Ar, Kr, and CO matrices at liquid helium temperatures *Physica* B **352** 383–9

[27] Dmitriev Yu A and Zhitnikov R A 1990 Ortho–para conversion in solid H_2 stimulated by atomic nitrogen impurities *Fiz. Nizk. Temp.* **16** 94
Dmitriev Yu A and Zhitnikov R A 1990 *Sov. J. Low Temp. Phys.* **16** 50 (Engl. Transl.)

[28] Dmitriev Yu A 2005 EPR spectra of deuterated methyl radicals trapped in low temperature matrices *Low Temp. Phys.* **31** 423–8

[29] Tinkham M 1964 *Group Theory and Quantum Mechanics* (New York: McGraw-Hill)

[30] Knight L B Jr and Steadman L J 1983 ESR investigations of H_2O^+, HDO^+, D_2O^+, and $H_2^{17}O^+$ isolated in neon matrices at 4 K *J. Chem. Phys.* **78** 5940

[31] Pollack G L 1964 The solid state of rare gases *Rev. Mod. Phys.* **36** 748–91
Malkov M P *et al* (ed) 1985 *Handbook on Physico-Technical Fundamentals of Cryogenics* (Moscow: Energoatomizdat)

[32] Haefer R A 1981 *Kryo-Vakuumtechnik* (Heidelberg: Springer)

[33] http://www.webelements.com/webelements/elements/text/C/radii.html

[34] Gordy W and Cormick C G 1956 Microwave investigations of radiation effects in solids: methyl and ethyl compounds of Sn, Zn and Hg *J. Am. Chem. Soc.* **78** 3243–6

[35] Poole C P Jr 1967 *Electron Spin Resonance* (New York: Wiley)

[36] Brooks S A, Luckhurst G R and Pedulli G F 1971 Thermal fluctuations in the nematic mesophase *Chem. Phys. Lett.* **11** 159

[37] Zhitnikov R A and Dmitriev Yu A 1995 Interaction of trapped metastable excited He atoms with solid noble gases, Ne, Ar and Kr, investigated by EPR *Appl. Magn. Reson.* **8** 457

[38] McConnel H M 1958 Free rotation in solids at 4.2° K *J. Chem. Phys.* **29** 1422

[39] Nielsen R D, Canaan S, Gladden J A, Gelb M H, Mailer C and Robinson B H 2004 Comparing continuous wave progressive saturation EPR and time domain saturation recovery EPR over the entire motional range of nitroxide spin labels *J. Magn. Reson.* **169** 129–63

[40] Dmitriev Yu A 2007 Structural formation and thermal relaxation of quench-condensed Kr films: effect on EPR spectrum of trapped hydrogen atoms *Low Temp. Phys.* **33** 493

[41] Ogurtsov A N, Savchenko E, Vielhauer S and Zimmerer G 2005 Excitonic mechanisms of inelastic radiation-induced processes in rare-gas solids *J. Lumin.* **112** 97
Ogurtsov A N, Masalitina N Y and Bliznjuk O N 2007 Kinetic study of inelastic radiation-induced processes in rare-gas cryocrystals *Low Temp. Phys.* **33** 519

[42] Rojas-Lorenzo G, Rubayo-Soneira J, Vigliotti F and Chergui M 2003 Ultrafast structural dynamics in electronically excited solid neon. II. Molecular-dynamics simulations of the electronic bubble formation *Phys. Rev.* B **67** 115119

[43] Jones L H, Ekberg S A and Swanson B I 1986 Hindered rotation and site structure of methane trapped in rare-gas solids *J. Chem. Phys.* **85** 3203

[44] Prager M and Langel W 1988 Methane in vapor-deposited argon—an inelastic neutron-scattering study *J. Chem. Phys.* 887995
Langel W, Schuller W, Knözinger E, Fleger H-W and Lauter H J 1988 Disordered phases in vapor-deposited rare-gases *J. Chem. Phys.* **89** 1741
Prager M and Langel W 1989 Rotational excitations of methane molecules in a nonequilibrium krypton matrix *J. Chem. Phys.* **90** 5889
Prager M, Amussen B and Carlile C J 1994 Methane in neon—nearly free rotation in a mismatched guest–host system *J. Chem. Phys.* **100** 247

[45] Cole T, Pritchard H O, Davidson N R and McConnell H M 1958 Structure of the methyl radical *Mol. Phys.* **1** 406–9
Ogilvie J F 1976 The planarity of the methyl radical *J. Spectrosc. Lett.* **9** 203–10
Marynick D S and Dixon D A 1977 Electron affinity of the methyl radical: structures of CH_3 and CH_3^- *Proc. Natl Acad. Sci. USA* **74** 410–3

[46] Deshman S 1964 *Fundamentals of Vacuum Technique* (Moscow: Mir) (Russian translation)